Multiple Sclerosis Disease Diagnosis and Prognosis in 3D FLAIR MRI using Deep Learning Network

Chaima DACHRAOUI (chaima.dachraoui@istmt.utm.tn)
University of Tunis El Manar, Higher Institute of Medical Technologies of Tunis
Aymen MOUELHI
University of Tunis, National Engineering School of Tunis
Amine MOSBEH
Tunisia Military Academy Fondek Jdid, National School of Veterinary Medicine Sidi Thabet
Wassim SLITI
Tunisia Military Academy Fondek Jdid, National School of Veterinary Medicine Sidi Thabet
Cyrine DRISSI
University of Tunis El Manar, National Institute of Neurology Mongi Ben Hmida
Basel SOLAIMAN
IMT Atlantique, Pays de la Loire, LaTIM UMR 1101, UBL
Salam LABIDI
University of Tunis El Manar, Higher Institute of Medical Technologies of Tunis

Research Article

Keywords: Brain, multiple sclerosis, 3D FLAIR, segmentation, detecron-2, chaotic attributes, diagnosis, prognosis

Posted Date: May 6th, 2022

DOI: https://doi.org/10.21203/rs.3.rs-1571528/v1

Multiple Sclerosis Disease Diagnosis and Prognosis in 3D FLAIR MRI using Deep Learning Network

Chaima DACHRAOUI [a,*], Aymen MOUELHI [b], Amine MOSBEH [c], Wassim SLITI [c], Cyrine DRISSI [d], Basel SOLAIMAN [e], Salam LABIDI [a]

[a] University of Tunis El Manar, Higher Institute of Medical Technologies of Tunis, Research Laboratory of Biophysics and Medical Technologies LR13ES07, Tunis, Tunisia

[b] University of Tunis, National Engineering School of Tunis, Laboratory of Signal Image and Energy Mastery LR13ES03, Tunis, Tunisia

[c] Tunisia Military Academy Fondek Jdid, Computer Science Department, National School of Veterinary Medicine Sidi Thabet, Tunis, Tunisia

[d] University of Tunis El Manar, Faculty of Medicine of Tunisia, National Institute of Neurology Mongi Ben Hmida, Tunis, Tunisia

[e] IMT Atlantique, Bretagne, Pays de la Loire, LaTIM UMR 1101, UBL, Brest, France

Emails: chaima.dachraoui@istmt.utm.tn*, aymen_mouelhi@yahoo.fr , aminemosbah@hotmail.com, wassimsliti1998@gmail.com , cyrine.drissi@fmt.utm.tn , basel.solaiman@imt-atlantique.fr , salam.labidi@istmt.utm.tn

Corresponding author: Chaima DACHRAOUI, Doctoral researcher
University of Tunis El Manar, Higher Institute of Medical Technologies of Tunis, Research Laboratory of Biophysics and Medical Technologies LR13ES07, Tunis, Tunisia
E-mail: chaima.dachraoui@istmt.utm.tn
Postal address: 9 Street Zouhair Eaasfi, Tunis 1006,Tunisia
Phone number: +33 07 58 74 27 02, +216 25 259 049

Abstract

Multiple Sclerosis (MS) is a chronic autoimmune disease that affects the central nervous system. It is characterized by the appearance of inflamed lesions. The diagnosis, as well as the prognosis of these lesions, are considered as tedious tasks and time consuming. The objective of this paper is to propose an automated method allowing to assist and detect MS lesions in 3D MRI acquisition. A deep learning network based on the Detectron-2 model has been used. The proposed model involves three main steps: preprocessing, feature extraction and MS detection. A database of 4500 images was acquired from the National Institute of Neurology Mongi Ben Hmida of Tunisia and was preprocessed in order to train the model. In the prognosis stage, chaotic features extracted from the segmented lesions are used in order to define pertinent clinical characteristics that will help neurologists to predict lesions progression in the majority of complicated cases. In the diagnosis stage, the proposed deep model achieves an average detection accuracy of 98% by evaluating the result on healthy and pathological images. Automatic segmentation results show that our proposed method has the ability to segment MS lesions with an average accuracy of 96.4%.

Keywords Brain, multiple sclerosis, 3D FLAIR, segmentation, detecron-2, chaotic attributes, diagnosis, prognosis.

1. Introduction

Multiple sclerosis is a chronic inflammatory disease of the Central Nervous System (CNS). It is characterized by the development of an inflammatory reaction against the myelin. Some neurons of the CNS are covered with membrane that isolates and protects the nerve fibers of the brain and spinal cord. This myelin sheath is essential to accelerate the conduction of nerve messages. In particular, it promotes the “salutatory” propagation of action potentials **[1].**

In 85% of cases, MS begins with a relapsing form but the evolution of the disease still extremely unpredictable. It can start with a wide variety of signs depending on the location of the demyelination plaques. The symptoms of the MS disease are varied: visual, motor, sensory, urinary, and cognitive and all depend on the location of the lesions in the White Matter (WM) of the CNS **[2].**

Moreover, multiple sclerosis is not a hereditary disease. In fact, in case of genetic predisposition, an interaction with environmental factors is necessary for the disease to occur. This variety can make diagnosis difficult; hence,

the importance of medical consultation whether abnormal neurological symptoms occur. In the majority of MS cases, lesions evolution cannot be predicted, and several forms may develop differently. Schematically, there are two types of evolutionary form: A form evolving by relapses and it is characterized by the appearance of new disorders in few days, which may completely regress spontaneously or after specific treatments (called relapsing-remitting multiple sclerosis). The second form is unless relapses and it is characterized by a progressive evolution (called progressive primary form) **[3].**

The MS diagnosis is based on a set of clinical arguments and the result of definite clinical neurological examination during the medical consultation, in particular: Lumbar puncture, which looks for signs of inflammation in the CerebroSpinal Fluid (CSF) in the central nervous system. The evoked potentials analyze the functioning of the CNS. Also, Magnetic Resonance Imaging (MRI) allows to visualize plaques within the CNS, to explore their evolution over time and to identify the regions of the brain affected by inflammation. The appearance of the lesions on the MRI can be used to determine whether they are recent (i.e., active) lesions or ancient lesions (i.e., scars). MRI is not only used for diagnosis but also for patients monitoring and evaluating their response to therapeutic treatment **[4].**

These three methods provide arguments in favor of the diagnosis. These examinations establish an earlier diagnosis and a therapeutic strategy adapted to each patient.

In our work, several problems are encountered in three distinct axis: MRI acquisition, manual detection and segmentation of MS lesions and MS prognosis. These problems are described in the following sections.

1.1. 3D FLAIR Magnetic Resonance Image Acquisition

Magnetic resonance imaging plays an essential role in the study and assessment of demyelinating diseases. The MRI scan is essential in MS disease diagnosis, although lumbar puncture and blood tests are not always part of the "diagnostic investigation". The main advantages of using higher magnetic field is to increase Signal-to-Noise Ratio (SNR) and the contrast-to-noise ratio which allow better spatial resolution of anatomical and pathological characteristics. In this section, the current sequences and techniques used in MS acquisition and the different steps made to establish a sufficient diagnostic **[5]** are described**.**

Before the appearance of 3D FLAIR acquisition, clinicians mainly based their evaluation on T2 FLAIR acquisition, where the whole brain appears as a hypo-signal and the lesions appear as a hyper-signal. The FLAIR acquisition facilitates the exact pointing on the MS lesions. Although, the intensity distribution of MS lesions and its overlap

with the Green Matter (GM), is due to the limited resolution of the image and the heterogeneity of the lesion **[6].** Hence, the main advantages of using higher magnetic. However, 2D FLAIR acquisition remains a slightly high SNR with a very high acquisition time. Furthermore, the use of this sequence does not allow the passage through the axes (axial, sagittal and coronal) and, subsequently, it does not allow to 3D reconstruction. Hence, the interest to attempt new acquisition, it is 3D FLAIR acquisition (Fig.1).

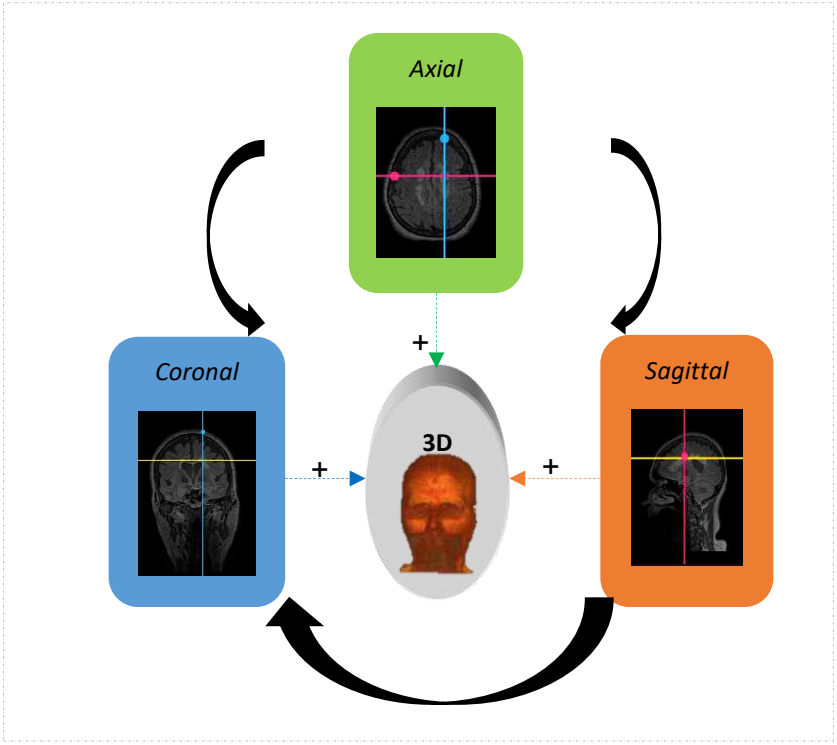

Fig 1. 3D FLAIR acquisition

This acquisition was developed in order to remedy all these inconvenients. In fact, the T1 sequence is purely used in morphological analysis and in the search for abnormal contrast enhancement. The images weighted T1 are anatomical images such that GM appears gray, WM white, CSF black and fat appears white. The T2-weighted sequences are used in content analysis: water, edema, inflammation. The contrast of the image is reversed compared to the T1 sequence: the GM is white, the WM is gray, the CSF is white and the fat is white (Fig 2). The FLAIR sequences are used for better differentiation between healthy and pathological tissues, especially in the periventricular regions. Due to the suppression of the CSF signal with a TE (i.e., repetition time) greater than T2, (i.e., this is a T2-weighted sequence, obtained by Inversion-Recovery, IR). For 3D FLAIR sequences, these are fast spin echo techniques with special modifications optimized for isotropic 3D imaging. The voxels generated by the 3D acquisition measure the same signal in each direction which makes it possible to have an equal image

resolution in any direction. It is a sequence useful in a wide range of clinical applications classified into two general categories: high resolution for isotropic images of complex anatomy (brain, inflammatory diseases), replaces several 2D acquisitions (spine, pelvis). 3D-fast (turbo) spin-echo acquisition is characterized by ultra-short echo spacing and a reduced flip angles with reasonable imaging times (5-10 min).

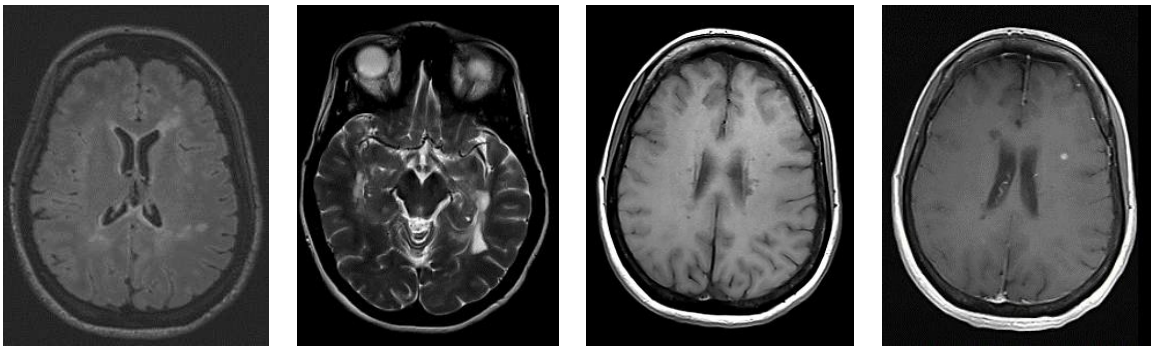

(a) **(b)** **(c)** **(d)**

Fig 2. Common sequences for MS disease: a) T1, b) T2, c) T2 FLAIR, d) 3D FLAIR

1.2. MS lesions diagnosis

The diagnosis of MS disease based on McDonald criteria (Table1) and the delineation of lesions (manually or automatically) **[7].** According to the current diagnostic criteria proposed by McDonald, revised in 2017, it is possible to diagnose MS dissemination in space and time using MRI **[8]** leading, thus to the necessity to segment the images in order to obtain a map of WM lesions.

The manual monitoring of MS plaques still remains a major problem and considered as a tedious task for the clinician requiring ~~a~~ high level of anatomy knowledge to identify the lesions and, also, sensitive to observer intra/inter variability. Furthermore, MS lesions segmentation is an essential task for quantitative analysis of the disease progression. Therefore, the conception of a robust model to automatically segment MS lesions is always of major interest of several authors working on neuroradiology, essentially to reduce the discordance between clinicians and to increase the accuracy of diagnosis.

Table 1. McDonald criteria for MS dissemination

Inactive plaque Signal	Hyper-signal T2 with net outlines Hyper-signal FLAIR Hypo-signal T1 Hyper-signal T1+Gd (plaques non enhanced)
Active plaque signal	Hyper-signal T2 with blurred outlines Hyper-signal FLAIR Hypo-signal T1 Hyper-signal T1+Gd

Several researches proposed semi-automatic segmentation methods, including the study of Dachraoui *et al*., **[9]** where the authors used mathematical morphology and active contour models to extract MS lesions. However, these methodologies still need improvement in terms of segmentation quality and implementation settings. Thus, different studies are based on the use of machine learning techniques to circumvent the problem of manual interventions. Shahab *et al.,* **[10]** proposed a novel Convolutional Neural Network (CNN) architecture for brain lesions automatic segmentation. They first used a specific filter sized 3x3 or 5x5 depending on the size of the lesions. In fact, it's hard to decide which filter will be the best for the detection and segmentation tasks. A Google Net launcher has been introduced to solve this problem by using pooling filters. The results showed that network performance in segmentation of MS lesions is enhanced following the integration of starter modules into the CNN architectures. Two evaluation criteria were used: the Binary Cross Entropy (BCE) and the Structural Similarity Index Measure (SSIM). The authors achieved a score of 93.81% on the public database ISBI-2015. Sergi *et al.,* **[11]** presented an approach based on a cascade of two 3D CNN. The first network is trained to be more sensitive by segmenting lesion voxels while the second network is trained to reduce the number of misclassified voxels from the first network. The proposed architecture tends to learn well from a small labeled database which can be of great interest in practice, given the difficulty of obtaining manual label annotations and the large amount of unlabeled magnetic resonance imaging. The authors evaluated the accuracy of their method on the public database MICCAI2008. The available entry methods are T1, T2 and FLAIR weighted MR Images. On MS clinical data, the approach showed a correlation index greater than 0.97. Francesco *et al.,* **[12]** proposed a fully convolutional, 3D U-Net-based deep learning approach for lesion and WM segmentation at 3T field MRI. In this study, the authors worked on T2 FLAIR and T1 MP2RAGE weighted images. They worked on a database of 90 patients with a total

of 728 and 3856 gray and white matter lesions. The proposed approach can achieve a detection rate of 76% for cortical and WM lesions with a false positive rate of 29% in comparison with manual segmentation.

1.3. MS lesions prognosis

Spatial and temporal evolutions are independent. Sometimes the patient relapses without indicating any new lesion on brain MRI which makes the evolution of this disease unpredictable and not defined even by a specific criterion. Evenly, unpredictable systems are not defined by equations since it changes in time and space (which is the case of MS disease). In fact, the prognosis of this disease "may" be defined and traced by systems and chaotic features as long as they share the same characteristics. In general, the MS lesion is geometrically simple, round or oval. However, the confluence and coalescence of several lesions, called signal anomaly, can be characterized by a chaotic growth **[13].**

Chaos theory is being applied in physical sciences field in order to understand the nature of random phenomena. Nevertheless, it appeared recently in medicine field to provide better understanding of certain physiological or pathological phenomena. This theory overturns any phenomenon based on hazard and disorder. The proposed theory has been used in cardiology for the prognosis of arrhythmias. In Varun *et al.*,**[14]** the authors used chaos on the ElectroCardioGram (ECG) as a diagnostic tool to assess the functioning of the heart in a non-invasive way. In fact, the ECG signal is non-stationary and non-linear in nature, since it contains several time-varying frequencies. The authors used the STFT technique to detect the R peaks and their frequency content. The sketched trajectories represent the flow of the system where each trajectory involves a sub region of phase space known as the attractor. An attractor presents the best preview given the initial conditions and the dimension of the delay. In order to validate their study, the authors used the physioNet database M-BArr DB, Ventricular Tachyarrhythmia database (VT DB) and the real-time database (RT DB).

Chaotic features have been also used in oncology. Denis *et al.,* **[15]** claimed that the evolution of cancer is highly different, unexpected and often unpredictable. To describe this evolution, the used mathematical approach is based on statistics and laws of probability. It is worthwhile to note that this approach has poorly characterized the dynamics of cancer. Chaos theory may provide a better understanding of these issues and was developed to study complex systems containing unpredictable components with high sensitivity to initial conditions (which is a new approach to cancer dynamics). Their study clarified the main points of connection between chaos and carcinogenesis, and they pointed out some promising research prospects, especially in radiotherapy.

The pathological mechanism of multiple sclerosis disease is unknown. In the literature, numerous studies have been discussed to understand its evolution. Among them, Akaishi *et al.* **[16]** have shown that dynamic cells presenting chaos are defined as lesions with chaotic growth. This may explain its evolution in the long or short term. Firstly, they adopted a discrete equation with non-linear dynamics systems to prepare a scalar quantity for the strength of pathogenic factors at the central nervous system that can lead to clinical relapses and cerebral atrophy. These functions ultimately represent a simple model specific to each lesions subtype: relapsing–remitting, primary progressive and secondary progressive. By applying chaos theory to three-dimensional acquisitions of the CNS, and by adjusting parameters, the authors were able to reproduce the nonlinear result of clinical evolution and explain the relapses in time and space. In order to demonstrate the accuracy of these results, this study remains to be compared with chaotic attributes extracted from the lesions more specifically.

2. Materials and Methods

Artificial Intelligence (AI) is the combination of algorithms formulated for the purpose of creating machines that have "almost" the same human skills **[17].** It's a technology which still seems distant and mysterious, however which had a constant presence in the medical imaging field. The proposed diagnostic approach, in this paper, is essentially based on supervised learning which is the most popular paradigm for machine learning. In fact, automatic detection of MS lesions is performed through deep learning using the supervised RCNN DETECTRON-2 model **[18]**. Since its release in 2018, the used model has become one of the most "widely" open source adopted for several works. The second generation of the library is "freshly" published, with important enhancements for research use.

Detectron-2 is a ground-up rewrite of Detectron. It is flexible and extensible, and able to provide fast training on single or multiple GPU servers. Its extensible design makes it easy to implement cutting-edge research projects without having to fork the entire codebase. We are working on Detectron2 due to the new models included such as Faster R-CNN, Mask R-CNN, RetinaNet, and DensePose; and the several new features including Cascade R-CNN, Panoptic FPN, and TensorMask. Moreover, by moving the entire training pipeline to GPU, Detectron2 is faster for a variety of standard models. Additionally, distributing training to multiple GPU servers is now easy, making it much simpler to scale training to very large datasets **[19].**

In this paper, the proposed method is essentially divided into two stages: diagnosis and prognosis stages. The step-by-step flowchart of the proposed method is presented in Fig. 3.

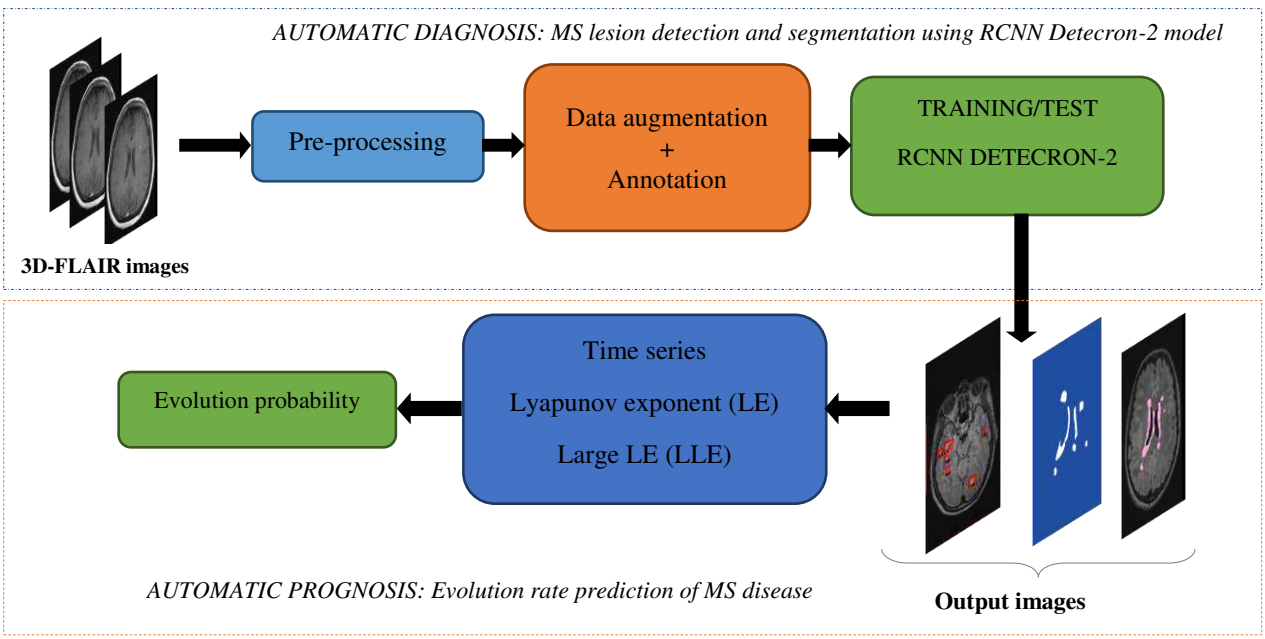

Fig 3. Flowchart of the proposed MS diagnostic and prognostic processes

2.1. MS diagnosis using RCNN Detecron-2 model

2.1.1. Dataset description

For the used data set, only on 3D FLAIR (known as SPACE in Siemens scan) axial acquisition sequences are considered in this study. This data is collected from the Neurological Institute Mongi Ben Hmida of Tunisia. The MR Images are acquired, with the DICOM (Digital imaging and communications in medicine) format, from a 3Tesla magnetic field MRI Siemens machine. Other details of the dataset population and acquisition parameters are summarized in Table 2.

Table 2. Dataset description and acquisition parameters

The studied Dataset	*Description*	*Number*
Patients	Pathological and healthy patients	150
Ages	Ranging from 12 to 80 years	Ø
Sex	Male and Female	Male : 122; Female: 118
MR acquisition type	3D FLAIR cerebral acquisitions	Pathological images : 4000 Health images: 500
Equipment modality	MRI 3Tesla, Siemens machine	
Transmit coil name	Body	
	TR=4500.0 ; TE= 395.0 ; TI= 1800;	

Acquisition parameters	Slice thikness=1mm ; Rows= 512; Columns=512; Flip angle=120; Pixel spacing= 0.488; Definition pixel image = [0 589]; Fov= 250*250; Coding schemed signator : DCM	Ø

2.1.2. Preprocessing pipeline

The proposed model undergoes preprocessing in two steps: contrast enhancement and artefacts removal steps. Indeed, in some cases, lesions appearing in "high intensity" are not clear enough to detect. Therefore, the histogram readjustment is first applied. This method is based essentially on the histogram of the image. In fact, histogram equalization is used to better distribute the intensities over the entire range of possible values, by "spreading" the histogram. Thereafter, this operation is of a huge interest for images for which all the pixels are of close intensity (or only a part) or have a low contrast. It consists of applying a transformation to each pixel gray level from the original image. This transformation is constructed from the cumulative histogram of the original image. This method is fast, easy to implement, and totally automatic (Fig.4).

After highlighting the lesions, the use of noise elimination filter is a mandatory process in medical image processing because of some artefacts that can affect diagnosis process. In this, considering that our images are affected by a Gaussian noise, which is, according to the bibliographic studies **[20],** the noise affecting the MR Image the most. Therefore, a 2D Gaussian linear model with 3x3 averaging filter kernel is applied (Eq. 1):

$$K = \frac{1}{9}\begin{bmatrix} 0 & -1 & 0 \\ -1 & 1 & -1 \\ 0 & -1 & 0 \end{bmatrix} \quad \textbf{(1)}$$

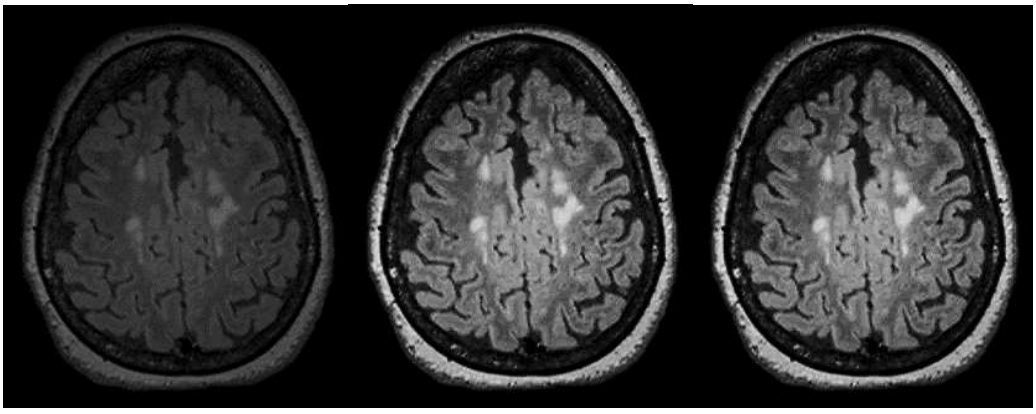

(a) **(b)** **(c)**

Fig 4. Preprocessing steps

a) Original image, b) Image contrasted by histogram equalization, c) Filtered image.

As can be noticed from Fig.4, the use of the 2D Gaussian reduced the effect of the additive Gaussian noise while preserving important details related to the regions of interest (i.e., lesions) which have already been highlighted due to the contrast adjustment.

2.1.3. Data augmentation

Acquiring a large dataset is always crucial and important for the performance of machine learning approaches, mainly Deep Models. Data Augmentation (DA) process increases the diversity of images used for training without actually having to collect new additional data. DA refers to the random application of various types of transformations to the images already existing in the dataset, see Table 3. Among the geometric transformation methods we cite the mirror reflection of the image on its vertical or horizontal axis. Also, the rotation of the original image "I" which consists in rotating the image around its center by mapping each pixel I(x, y) at any angle of rotation **[21].** According to the conducted experiments, setting +10 degrees or -10 degrees rotations which are really large enough to generate new invariant images. Cropping is another method of augmentation. The latter consists of resizing the image to a single size. This size is done by multiplying the image by a factor that varies from 0 to 2. If the factor is less than 1, the size of the image will decrease and *vice versa*.

Table 3. Data augmentation

Type of process	*Description*
Mirror reflection	Horizontal and vertical
Rotation	Horizontal degrees 10 vertical degrees 10
Contrast	[20 200]
Gaussian blur	$\delta = 0.5$

The DA operations were applied before the training and validation process. By this step we have increased the size of our image dataset from 4500 images to 5000 images using this process.

2.1.4. Training dataset annotation

Before starting this step, our database is first divided into two parts: healthy and pathological patients. We have divided pathological patients into 3 groups: training, validation and test (Fig.5).For the test stage, the 10% of the pathological images are used as well as the totality of all the healthy images devoid of MS lesions.

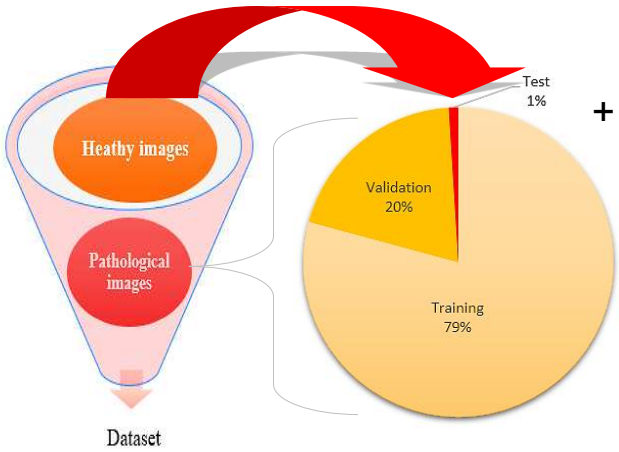

Fig 5. Dataset distribution

After dividing the data, we pass to labeling the pathological images using a specific tool in which we assign to each MS lesions ~~a~~ well-defined characteristics. This task requires special technical skills and requires the assistance of neuroradiological clinicians, especially in the event of abnormal signals. However, it consumes a lot of time since the lesions are sometimes of difficult visibility or very close to each other. Labeling is of great importance for machine learning algorithms. The data must be well structured and labeled in order to properly train and deploy the used model. For this step, the VGG Image Annotator (VIA) was used which is an open source software based on HTML, JavaScript and CSS, and is very useful for both academic projects and commercial applications. MS lesions are annotated manually with the help of three experimented clinicians. This tool generates .Json files that contain the coordinates of every mask image, these coordinates (ground-truth) mask images are then employed to compute the reverse loss at training and validating stage of our model.

2.1.5. Automatic MS detection and segmentation using DETECTRON 2 Model

In this part, the deep neural network model applied in our work to detect and to extract MS lesion regions in 3D FLAIR images is described. The proposed model is based on the DETECTRON-2 which is the next-generation open-source object detection system. The repo can be used and trained with various state-of-the-art models for detection tasks such as bounding-box detection, instance and semantic segmentation, and person key point detection (it is built using Pytorch). The EfficientDet is an object detection model created by Google brain team. It is a new neural network design for an object detection task. It already beats the RetinaNet, Mask R-CNN, and YOLOv3 architecture. Also, the architecture of EfficientDet employs the ImageNet pretrained EfficientNet as the backbone of the network. The EfficientDet purposes some new optimization techniques to improve the efficiency

as: BiFPN and a new Computational Scaling technique. In fact, Detectron2 is the combination of these two networks Detectron and RCNN Mask.

The mask R-CNN is conceptually simple: Faster R-CNN has two outputs for each candidate object, a class label and a bounding-box offset. In this stage we add a third branch delivering the outputs of the object mask. Thus, mask R-CNN is a natural and intuitive idea. But the additional mask output is distinct from the class and box outputs, requiring the extraction of much finer spatial layout of an object. Next, we introduce the key elements of Mask R-CNN, including pixel-to-pixel alignment, which is the main missing piece of Fast/Faster R-CNN.

In the Fully Convolutional Network (FCN) developed by Long *et al.,* **[22]** the last fully connected layer is replaced with a fully convolutional layer. This major improvement allows the network to have a dense pixel-wise prediction. A novel approach that uses Detectron is, thus, proposed in this study. There is no need for grayscale conversion or binary segmentation in our proposed method. The entire process is fully automated, quick, and precise. The architecture of the proposed model is summarized in Fig.6. To train our models, we first adopt these models for MS lesions identification. By setting the class number of each of them as one of two: MS lesions, no MS lesions, each model predicts two values as well as the class probabilities for each anchor box.

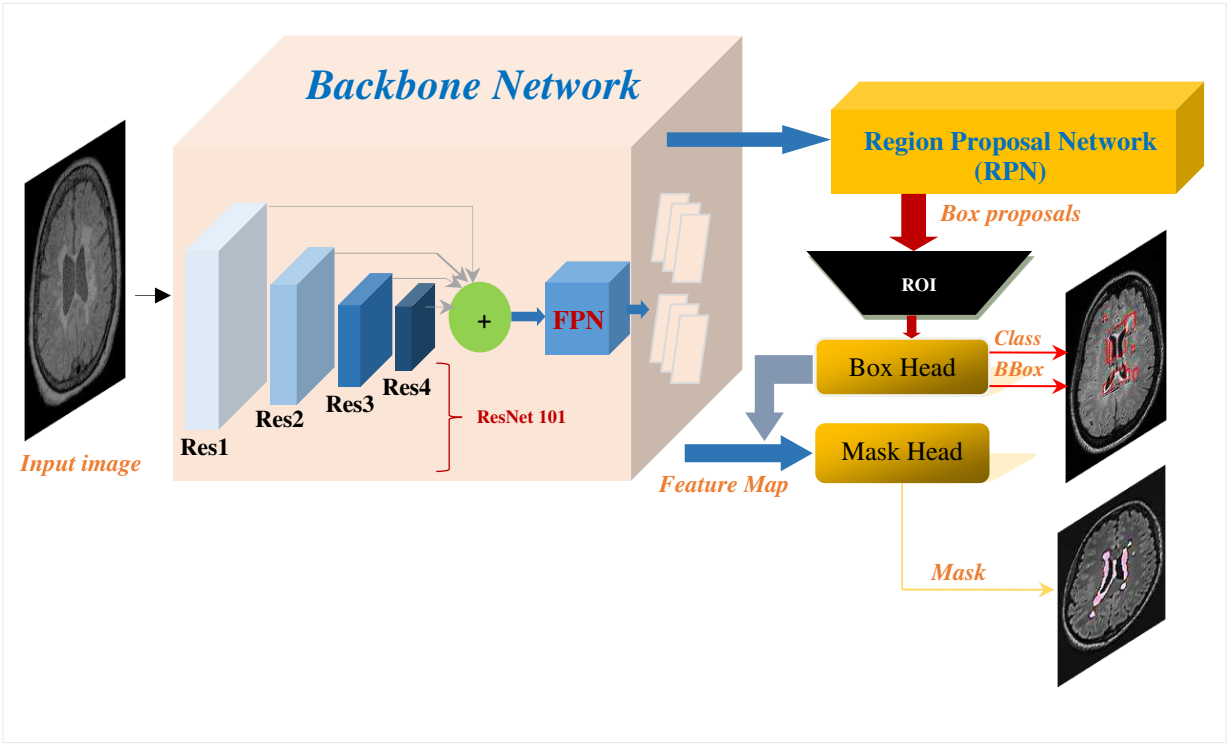

Fig 6. Detectron-2 architecture used for MS detection

For training, we use 4500 annotated lesions images and 500 for testing. During training, the loss and moving average loss at each step is recorded. Training is conducted through 3500 steps and the use a learning rate of 0.005 is considered. Every 125 steps, the weights are recorded, and modem performance is evaluated. The moving average of the loss function is used to represent the value of the loss function. The mask-RCNN model employs this configuration. This is due to the fact that deep features can be obtained when going deeper; moreover, spatial location information is also lost when going deeper. This means that the outputs from shallower layers have more location information. It is worthwhile to notice that the combination of both is appealed to the result. The MASK R-CNN model is a powerful for object localization. It is able to predict and segment bounding boxes for MS lesions inside the predicted boxes. The configuration of the proposed model is summarized in Table 4.

Table 4. Configuration of the proposed model

Model configuration	
Classes number	2 (MS or not MS)
Network backbone	ResNet_101
Activation function	(ReLu, Linear)
Dimension of input image	[256x256]
Learning rate	0.005
Train rols/image	125
Epochs	100
Batch size	5000
Kernel weight initializer	Uniform

2.2. MS prognosis *based on chaotic features*

Chaos theory is being applied in physical sciences fields in order to understand the nature of random phenomena. Nevertheless, it appeared recently in medicine field in order to provide better understanding of certain physiological or pathological phenomena. This theory overturns any phenomenon based on hazard and disorder **[23].** In fact, a chaotic system presents extreme sensitivity to initial conditions. This means that the less the difference in the beginning of the phenomenon, or the less the inaccuracy, even minimal, in the measurement of the initial parameters is, then, amplified in such proportions that the state reached be completely unpredictable. Sometimes systems remain generally random to predict their future except in statistical terms but their behavior can be quantified by a series of well-defined parameters. Indeed, there are three types of models: deterministic; stochastic and chaotic deterministic. For deterministic models, their evolution is determined by their current state.

Therefore, if the current state is determined, its past can be reconstructed and its future can be predicted. For stochastic models, the evolution is determined by probabilistic studies. For the 3^d model, i.e., chaotic deterministic, the evolution is determined only by its current state and we cannot predict its future **[24].** Determinism creates its own hazard. This is indeed the case of the MS disease. We only know the current state of the patient either in its recurrence or in its recovery.

Predictive calculations is based on the following features: Phase Space (PS), Time Series (TS), calculation of Lyapunov Exponents (LE) and fractal dimension estimation (D). The Phase Space PS(x,y), whose coordinates are the components of the state, is used to represent the evolution of a dynamical system such that x corresponds to the different degrees of liberty as a function of y, i.e., movements of the system. All systems that evolve towards a stationary equilibrium position can be represented by a fixed point in PS.

The prediction is essentially based on TS for quantitative analyzes. A time series with discrete time is a finite sequence (x_t); $1 \leq t \leq n$, where t represents the time. It includes generally several elements: the bias which represents the evolution of the series in long-term; the seasonality that characterizes the repetitive evolution regularly every year; and the stationary component which describes series evolution in the short-term, Eq.2.

$$x_t = T_t + S_t + \in_t \text{ Where, } t \in \{1, \ldots, n\} \quad \textbf{(2)}$$

Where T_t, resp. the bias, S_t, denotes the seasonality, ϵ_t resp. the stationary.

Although, the system course can be affected by white noise, impacting, thus, the TS representation. White noise is a low-intensity process that is a sequence of independent random variables (x_t), of constant expectation and variance. If the expectation is zero, the white noise is called centered, and if the random variables are Gaussian, the white noise is called Gaussian. Therefore, filtering as pre-processing provides a more appropriate procedure for later stages. A fractal structure is a structure that is unpredictable and characterized by self-similarity, structure emergence, and topology. The fractal structure is defined by a particular dimension between 1 and 2 or between 2 and 3, e.g. the triangle of Von Kosch which has a dimension equal to 1.26 **[23].**

The analysis and modeling of phase portraits permit the study of the conditions of stability and instability of the system as well as the transition to a chaotic state by the appearance of fractals. To have the geometric support of chaos is therefore to have its signature. The presentation of the chaotic non-linear system passes through two fractals (Fig.7), it depends on its characteristics.

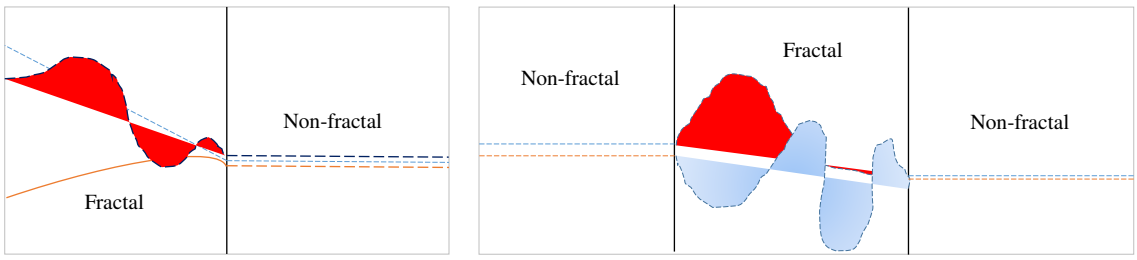

(a) **(b)**

Fig 7. Fractal transition: a) one transition; b) two transition

More generally, when a fractal with “internal similarity", the part of the structure (i.e., the fractal object) enlarged by a factor “k”, gives the entire fractal constructed of “N” replicas of this part, its fractal dimension is given in Eq.3 :

$$D = \frac{\ln(N)}{\ln(k)} \tag{3}$$

If the object presents locally internal similarity, we consider that the structure has a side “ε” and to obtain the value of “1” we apply an enlargement of " $1/\varepsilon$". The number of squares necessary to cover the side is denoted “N_ε”, its fractal dimension will then be small, Eq.4:

$$D \approx \frac{\ln(N_{\in})}{\ln(\frac{1}{\varepsilon})} \tag{4}$$

More formally, we will obtain the fractal dimension by letting “ε” tends to zero. Denoting that dim_F the fractal dimension of an object “F” we therefore obtain:

$$\dim_F = \lim_{\varepsilon \to 0} \frac{\ln(N_t)}{\ln(\frac{1}{\varepsilon})} \tag{5}$$

In fact, the degree of sensitivity to the initial conditions quantifies the chaotic character of the system. It is evaluated by the numerical values of the Lyapunov Exponents, LE. The LE spectrum is calculated from TS. Fig.8 illustrates the convergence and divergence of Lyapunov exponents in a 2-dimensional system.

The first exponent of the series is given by Eq.6:

$$\lambda_1(t) = \frac{1}{t} \ln \left\| \frac{u_1(t)}{u_1(0)} \right\| \tag{6}$$

Where $\lambda_1(t)$, resp. the first exponent $u_1(t)$, denotes the first divergence, $u_1(0)$ resp. the first point.

And the second by Eq.7:

$$\lambda_2(t) = \frac{1}{t} \ln \frac{v_2(t)}{v_2(0)} - \lambda_1 \tag{7}$$

Where $\lambda_2(t)$, resp. the second exponent $v_2(t)$, denotes the second divergence, resp. the second point.

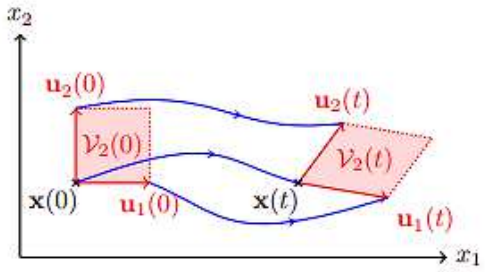

Fig 8. Illustration of Lyapunov exponent trajectory in 2D

If we consider $x(0)$ as the real initial position of the system and $x(0)+u(0)$ as the measured initial position of the system, then $u(t)$ is the difference at time t between the real trajectory and the trajectory calculated from the measured position. Thus, if $\lambda_1 < 0$, the distance between the two trajectories tends exponentially towards 0. Conversely, if $\lambda_1 > 0$, the calculated trajectory deviates exponentially from the real trajectory and we can quickly predict nothing more about the evolution of the system.

In fact, after detecting MS lesions in the diagnostic step, their prognosis is then conducted. In the case where the signal is generated by a linear source, the Fourier spectrum can provide relevant information. On the other hand, for signals generated by non-linear sources, their characterization by a Time Series (TS) is strongly recommended. Therefore, time series analysis extracted from lesions may provide a more appropriate solution **[25].** TS is defined as the Euclidean distance of each point of the contour of the lesion with respect to its center of gravity. Therefore, the number of sampling points differs depending on the lesion geometry.

Fractal geometry provides a mathematical model for complex objects which are too complex to possess characteristic sizes and to be described by traditional Euclidean geometry. Self-similarity is an essential property of fractal in nature and may be quantified by a Fractal Dimension (FD).

The box-counting approach is one of the frequently used techniques to estimate the FD of an image; therefore for fractal dimension calculation, the box counting method **[26]** is considered in this study**.** This method is based on

dividing the given lesion into square boxes with uniform sizes and the same process will be repeated into having more little squares (Fig.9).

The fractal dimension of a bounded set "A" in the Euclidean n-space is defined as shown in Eq.8:

$$FD = \lim_{r \to 0} \frac{\log(N_r)}{\log(\frac{1}{r})} \quad \textbf{(8)}$$

Where "N_r" denotes the number of squares necessary to cover the side, and "r" refers to the side.

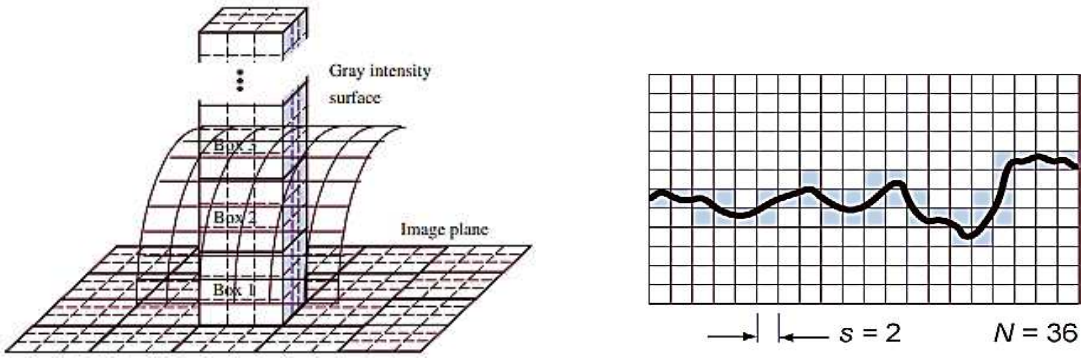

(a) **(b)**

Fig 9. Calculation of fractal dimension in the phase space
a) Box counting architecture, b) FD estimation [27]

Lyapunov Exponent (LE), extracted from TS, determines the stability's properties and the degree of stochastic trajectories. They are related to the expansion and contraction of various directions in Phase Space (PS). Estimating the spectrum of large Lyapunov (LLE) is extremely interesting because it encapsulates, in an intuitive form, certain dynamic information contained in the data. However, if we have dynamic information, Lyapunov values will automatically change. In this step, we will only base on the large value of the LE.

3. Results and Discussion

The implementation of this model was performed using Intel(R) Core (TM) i7-9 700 CPU 3 GHz with 16Go RAM memory, and graphical card NVIDIA GeForce GTX 1650 SUPER. Throughout the development of the proposed approach, a specific software and hardware have been used. For the software we have used Anaconda which is a free and open source Python application for the development of data science and machine learning applications.

Anaconda was not chosen at random but rather for its utility while offering powerful functionality. We installed "Anaconda Prompt", which is a console, similar to IDLE (Integrated DeveLopment Environment) which was originally available in Python. The advantage of this environment, it allows libraries to be installed in order to use them in our proposed method. Also we have used Jupyter Notebook, which is an open source web application allowing to create and share live codes, equations, visualizations and narrative texts.

Our own use has included data transformation, numerical simulation, statistics modeling, data visualization and machine learning. In order to boost the tensor calculations necessary for the proposed method, we have also used PyTorch. It is an open source software library for Torch-based machine learning developed by Facebook. It was chosen due its stability. It includes high level features such as the computational tensor (similar to NumPy) with strong GPU acceleration.

3.1 Diagnosis

The effectiveness of the proposed model diagnosis takes place on 3D FLAIR axial MR Images dataset. It contains 4500 images between pathological and healthy patients. We applied pre-processing such as noise reduction and contrast adjustment (Fig.10). These improvements were based primarily on the histogram of the original image. Then we applied the data augmentation in order to increase the diversity of data without actually having to collect new data.

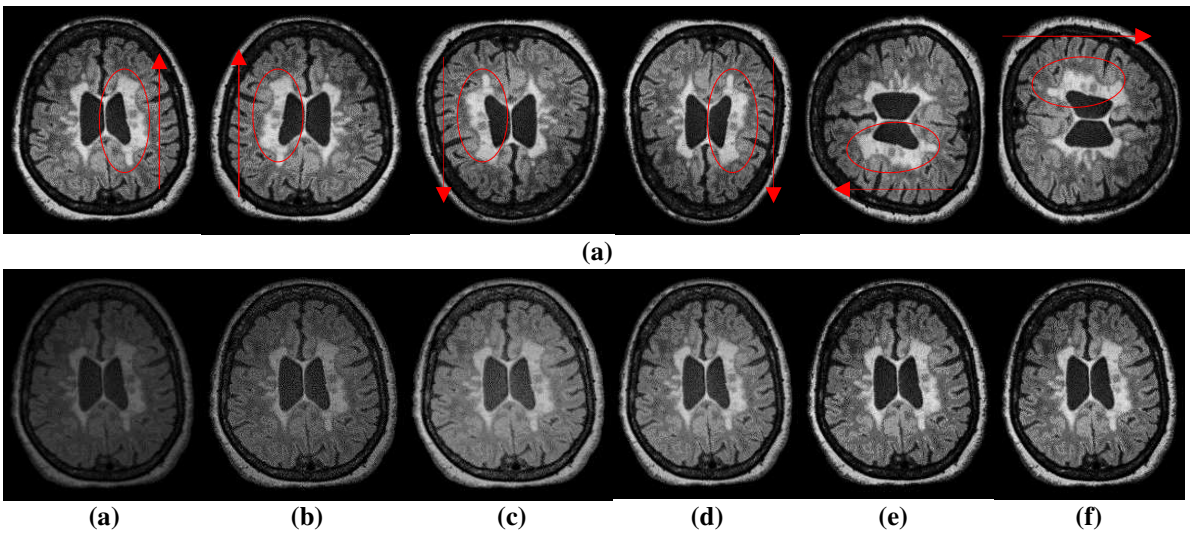

Fig 10. Data augmentation operations:
Row1: DA with possible rotation; Row2: DA based definition adjustment
a) Original image [0 255]; b) definition adjusted [10 255]; c) [20 255]; d) [30 255]; e) [50 255]; f) [90 255]

As can be noticed from Fig.10, from a single image, several new images can be generated by applying a simple reflection by mirror effect. Furthermore, changing the contrast interval of the original image may generate new images.

For the data annotation phase, we have used VGG-annotator due its several advantages. Running the model at the first use, a very low precision has been noted. Thus, other pre-processing was applied on the dataset to improve the model accuracy described in Table 5:

Table 5. Proposed preprocessing improvements

Proposed improvements
1. Down sample the image size to 520 x 520 for faster practice.
2. Verify, a second time, the labeling in the data annotation phase. Indeed some misplaced regions was founded, therefore a few regions in a more precise way was refined.
3. Remove all images that have a PSNR less than 60
4. Reformulate the dataset annotation from JSON form to CSV format to use both of them.
5. Use image augmentation (flips, rotations, etc.) to increase the size of the training set and balance out the classes.

For the annotation we used these characteristics (Fig.11). The labeling characteristics of MS lesions have been described in the previous section. Note this step is done manually.

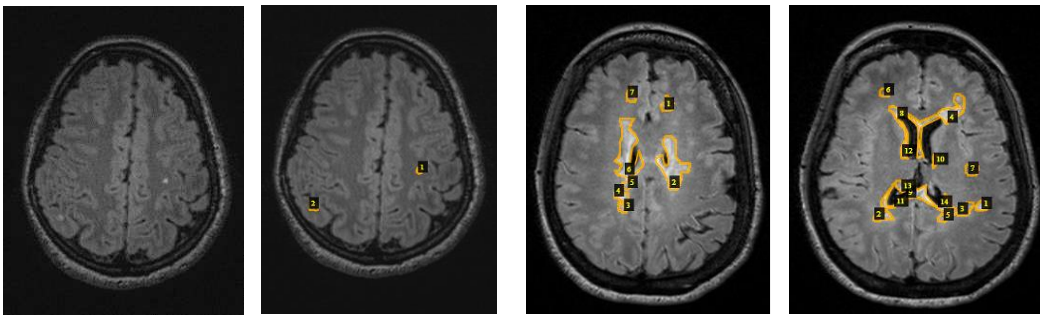

(a) **(b)**

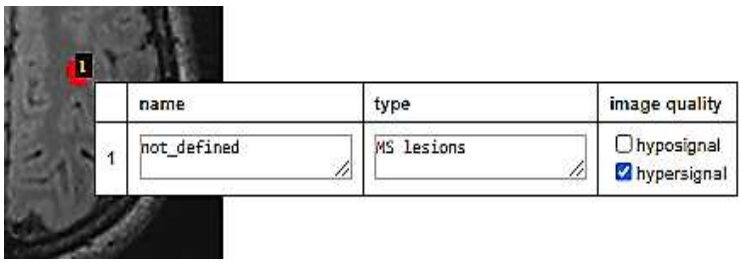

(c)

Fig 11. Data labelling using VGG annotator:
a) Original image; b) Data labelled; c) Labelling characteristics

As can be seen in Fig.11, the use of manual annotation requires a high level of anatomical knowledge. Which we can have one or two focal lesions, or minimal dispersed lesions.

After labeling the input images, deep learning approach is applied based on the detecron-2 architecture combined RCNN mask. The experiment approach was performed under deep learning frameworks of Keras and Tensor flow. The images were used with a batch size of 5000, and the value of learning rate was set to 0.005. We have set 100 epochs for training, with 432 steps in each epoch, after that the model starts to overfit and have put layers to all instead of heads to have more accuracy.

This model is trained using an optimization process that requires a loss function to calculate the model error. The Cross-entropy and mean squared error are the two main types of loss functions that has been used in the training process. The loss function has an important role in that it must faithfully distill all aspects of the model down into a single number in such a way that improvements in that number are a sign of a better model **[28].** It is used to evaluate and diagnose model optimization only.

The loss values in the training model are presented in Fig.12. The proposed model has four losses. First, we will have three functions corresponding to the fact of having three outputs: boxes, masks and classes:

- The Loss-BOX-reg for region detection. It is a loss that measures how close the bounding box predicted by the model is around the actual object;
- The Loss-CLS is a loss that measures the classification accuracy of each predicted bounding box;
- The Loss-RPN-cls for how well RPN locates objects. Finally,
- The whole set is evaluated by the TOTAL Loss which is a combination of all the losses.

Fig. 12 illustrates that the loss is a decreasing function by updating the synaptic weights of the network and the training and validation loss of the images sample batches during the optimization process.

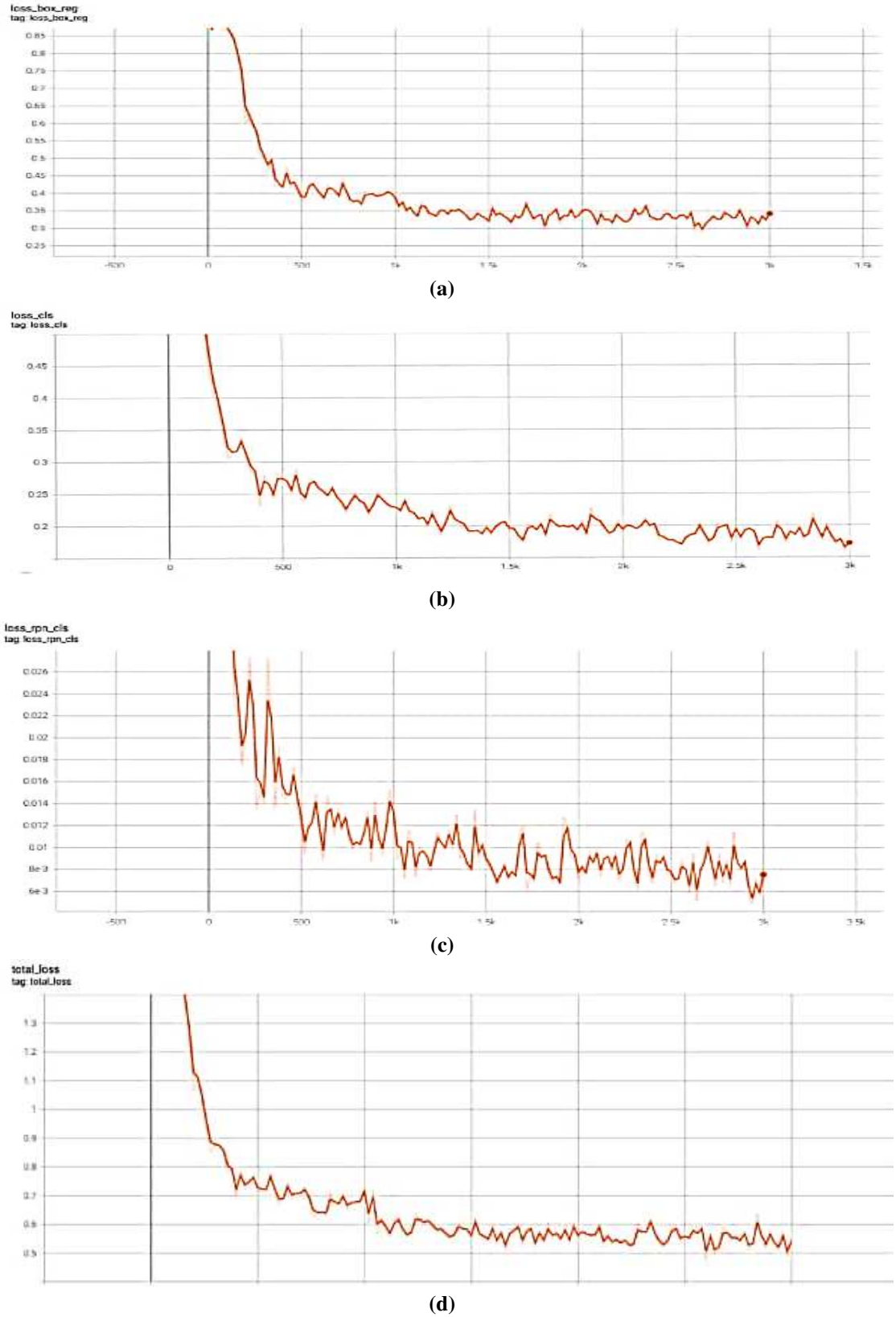

Fig 12. Evaluation of losses values during the training process: a) loss-BOX-reg for region detection, b) loss-CLS for classification, c) loss-RPN-cls for objects location, d) TOTAL loss for all losses

Figure.13 present the results of lesions detection by a red quadrant with their probability of membership.

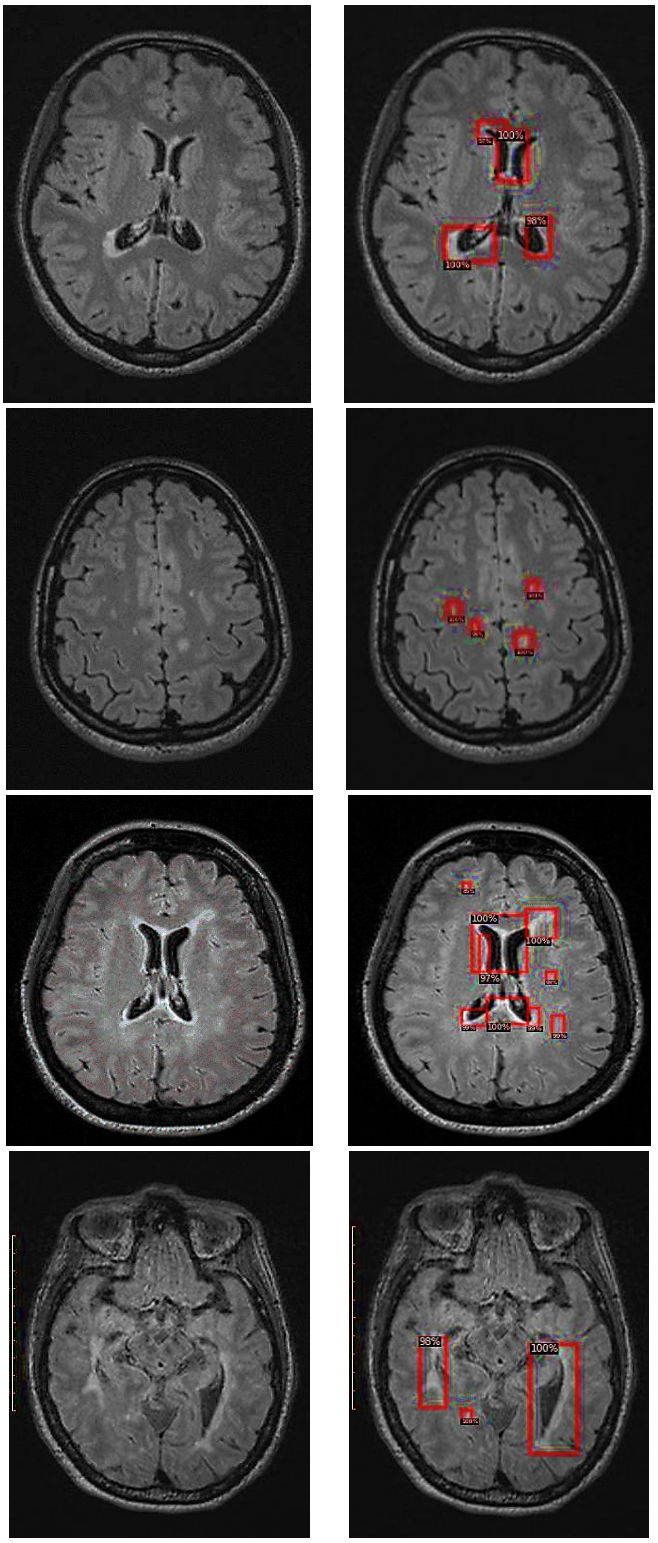

(a) **(b)**

Fig 13. Model detection results: a) Original image; b) Detection results

As can be seen in Fig.13, the probability according to the results varies between 98% and 100%. Indeed, it is the first output of the proposed model (i.e., this is the detection part).

During the optimization process, by updating the synaptic weights of the network and the training and validation loss of the sample batches of images, the loss function is a decreasing function. Therefore, from these experiments with epochs number = 100 and a loss function of the training and validation set is less than 1.30, these results clearly prove that the training model performs well and sound promising.

The multi-task loss function of the MASK RCNN combines the loss of classification, localization and segmentation mask is given in Eq. 13:

$$L = L_{\max} + L_{loc} + L_{seg} \quad \textbf{(13)}$$

Where $L_{\max}$ denotes the region detection, L_{loc} the objects location, and L_{seg} the loss-CLS for classification.

In the test phase, the model is evaluated using healthy and pathological images. In fact, as a result, a lesion is surrounded by a quadrant with the probability that this plaque is an MS lesion (Fig.13).

This model was adopted following segmentation problems fixed by clinicians. In fact, with color segmentation, two close lesions are colored as a one lesion. However, with the quadrant model, they appear as two different lesions (Fig.14). It is worthwhile to be noted that we are not in the case of ischemia or stroke lesions, one or two large clear lesions, but the MS lesions are small, glued to each other, and scattered everywhere in the white matter.

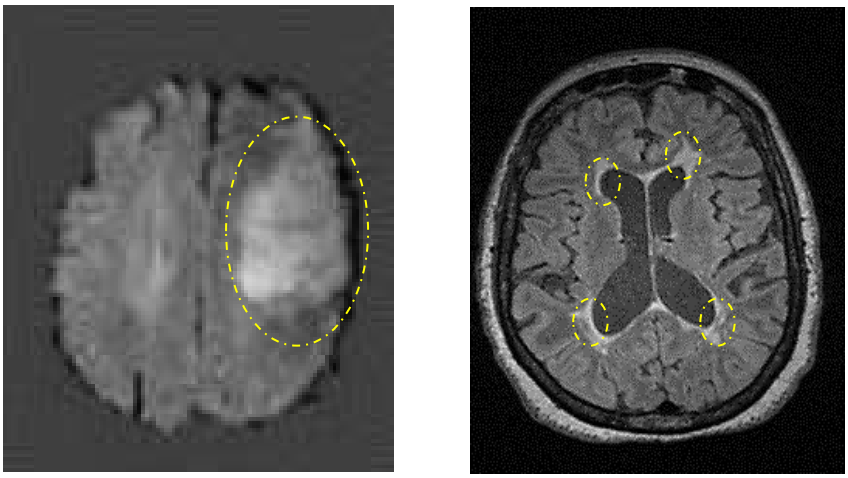

(a) **(b)**

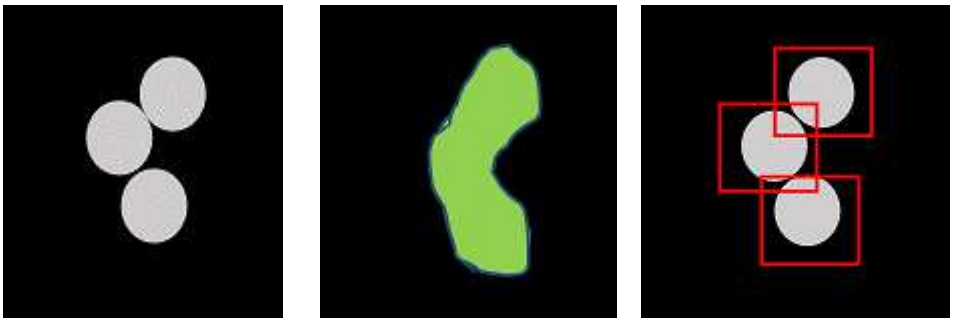

(a) **(b)** **(c)**

Fig 14. Row 1: Difference between lesions Row 2: Difference between detection and segmentation a) Stoke lesions, b) MS lesions; a) lesions, b) segmentation, c) detection

To evaluate the performance of the proposed detection and segmentation model, ACCruacy (ACC), Sensitivity (Sens), Specificity (Spec), Dice Similarity Coefficient (DSC) and the Positive Predictive Value (PVV) where considered. These measurements are defined as shown in Eq.14-18:

$$ACC = \frac{TP + TN}{(TP + FP + FN + TN)} \times 100 \quad \textbf{(14)}$$

$$Sens = \frac{TP}{(TP + FN)} \times 100 \quad \textbf{(15)}$$

$$Spec = \frac{TN}{(FP + TN)} \times 100 \quad \textbf{(16)}$$

$$DSC = \frac{2TP}{FP + 2TP + FN} \quad \textbf{(17)}$$

$$PPV = \frac{TP}{TP + FP} \quad \textbf{(18)}$$

These metrics is described in Table 6.

Table 6. Metrics description

Metrics	*Description*
True Positive: TP	The prediction which the lesion area, and the prediction are correct
True Negative: TN	The prediction is not the MS lesion area, and the prediction is not correct
False Positive: FP	The prediction for the lesion area, and the prediction is not correct
False Negative: FN	The prediction is not the MS lesion area, and the prediction is not correct

The proposed metrics are applied in the two outputs of the proposed model; segmentation and detection which are discussed in Fig. 15.

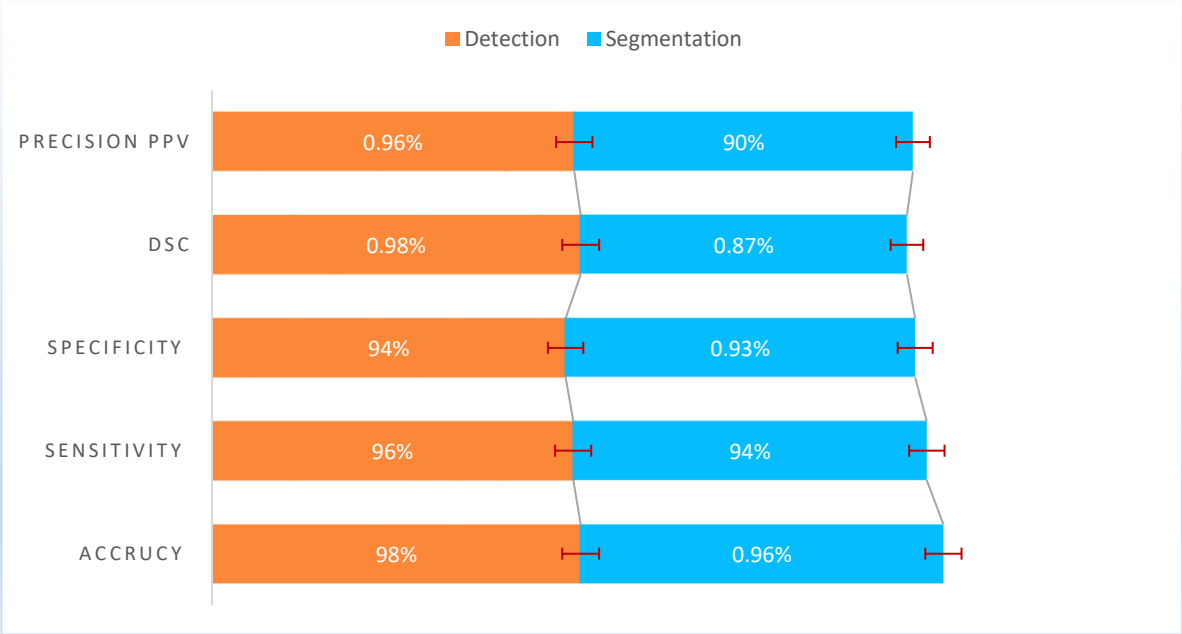

Fig 15. Segmentation and detection results

Figure.15 illustrates that the detection results are higher than the segmentation results. These results are due to the signal anomaly and the close dispersion of the lesions.

The obtained results are compared to other methods from the literature**.** A quantitative comparison of the methods reviewed is discussed. Although several methods for automatically segmenting MS lesions have been proposed in recent years, none of them is widely used in clinical practice. Thus, this task still encounters many technical problems and challenges.

Roy *el al.* **[30],** the authors used the "ISBI 2015" public database with 3D acquisitions containing MR images with MS lesions. The model turned in artificial intelligence is the semantic wise model. For Valverde *et al.*, **[31, 32],** in 2017, the authors used the public database "MICCAI 2008" and worked on 3D acquisitions. In 2019, furthermore,

the authors tested the same model on 3D acquisitions from the "ISBI 2015" public database. An additional study was also discussed, the model presented by Aslani *et al.* **[33]**, on 2D acquisitions of the public database "ISBI 2015" with the Semantic wise architecture.

The results are presented in the following figure (Fig.16) as well as a description of the database used by the discussed studies (Table 7).

Table 7. Compared results obtained with anterior studies

Database	*Subjects number*	*MRI sequences*	*MRI Scan*	*Training set: test set*
ISBI 2015	19	T1, T2, PD, FLAIR	Philips 3T	5 : 14
MICCAI 2008	45	T1, T2, FLAIR	Siemens 3T	20 : 25
Proprietary	150	T1, T2, PD, FLAIR	Siemens 3T	5000 : 100

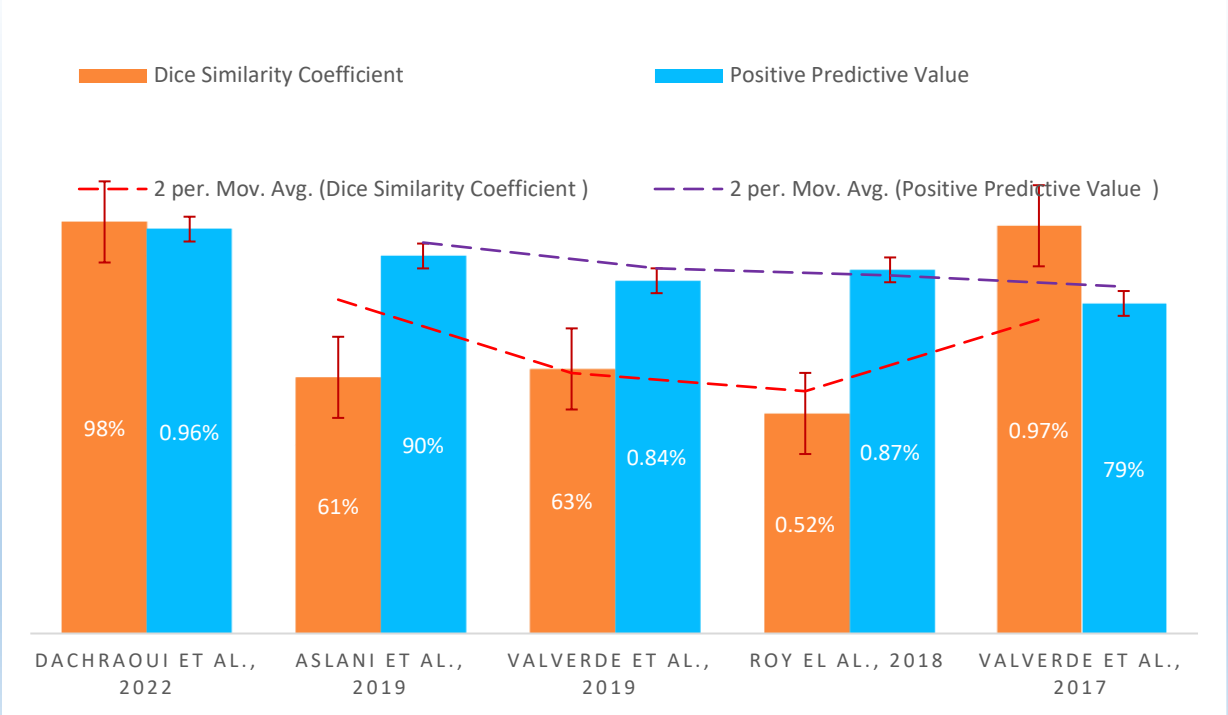

Fig 16. Comparative study

The results of the comparative study presented in Fig.16, demonstrates that the model proposed in this paper guarantees the best precision values reaching 98% and 96.3% which proves the robustness of our proposed approach. Previous authors used a public databases with a fairly small number of images for the training process. Contrary to our case, a large proprietary database collected with high resolution, dataset was used for the training, the validation, and the test.

The second output is dedicated for masks and classes (Fig.17) as these two outputs were superimposed on the original image by a different color (the segmentation part in Fig.18).

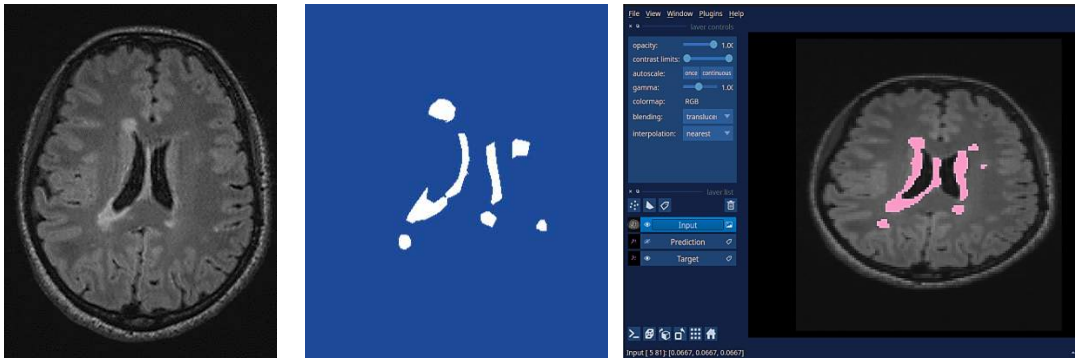

(a) **(b)** **(c)**

Fig 17. MS lesions segmentation: a) Input image, b) mask of MS lesions, c) output image

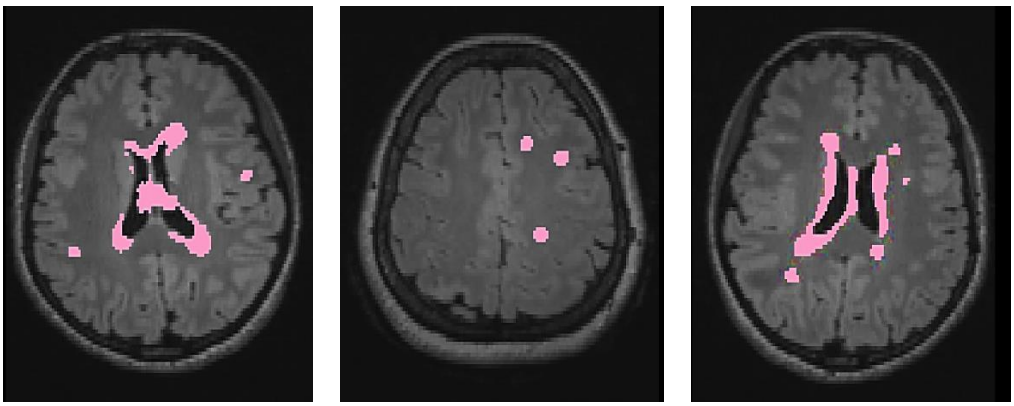

Fig 18. MS lesions segmented

3D FLAIR acquisition was chosen due to its PSNR compared to T2 FLAIR acquisition. This fact was verified by a quantitative study applied to a set of 300 images. The results shows that 3D FLAIR has the lowest error value (MSE), and the highest PSNR value compared to T2 FLAIR acquisition.

$$MSE = \frac{1}{MN} \sum_{0}^{M-1} \sum_{0}^{N-1} \left\| f(i,j) - g(i,j) \right\|^2 \quad \textbf{(9)}$$

$$PSNR = 20\log_{10}(MAX_f \frac{1}{\sqrt{MSE}}) \quad \textbf{(10)}$$

Where, "*f*"is a 3D FLAIR image, "*g*" is T2 FLAIR image and "MAXf" is the maximum possible luminance; "m" represents the numbers of pixels rows of the images and "I" represents the index of that row. "N" represents the number of pixels columns of the image and, finally, "j" represents the index of that column.

Although the MR Images acquisition in DICOM format was "normally" with high quality and resolution due to the higher intensity of the magnetic field (3T), but they are always accompanied by degradations and distortions, associated to the acquisition coil and cables, which are harmful for interpretation process. The MR Image is more affected by the Gaussian noise that will be misclassified and poorly segmented in the next step**.** Furthermore, as discussed in section 2.2, the system can be affected by a white noise which its random variables are Gaussian; hence, the benefit of filtering. We have used a median filter that combines both an effective suppression of impulse noise and the conservation of sufficiently important details. The choice of the filter was chosen by empirically comparing the results of the different types of filter applied to the original image. The comparative study used the criteria mentioned above. These criteria are calculated between the original and the filtered image (Fig.19). Indeed, the noise can't be materially observed with a naked eye, hence, the interest of first adding a configurable noise in order to accentuate the effect of the Gaussian noise.

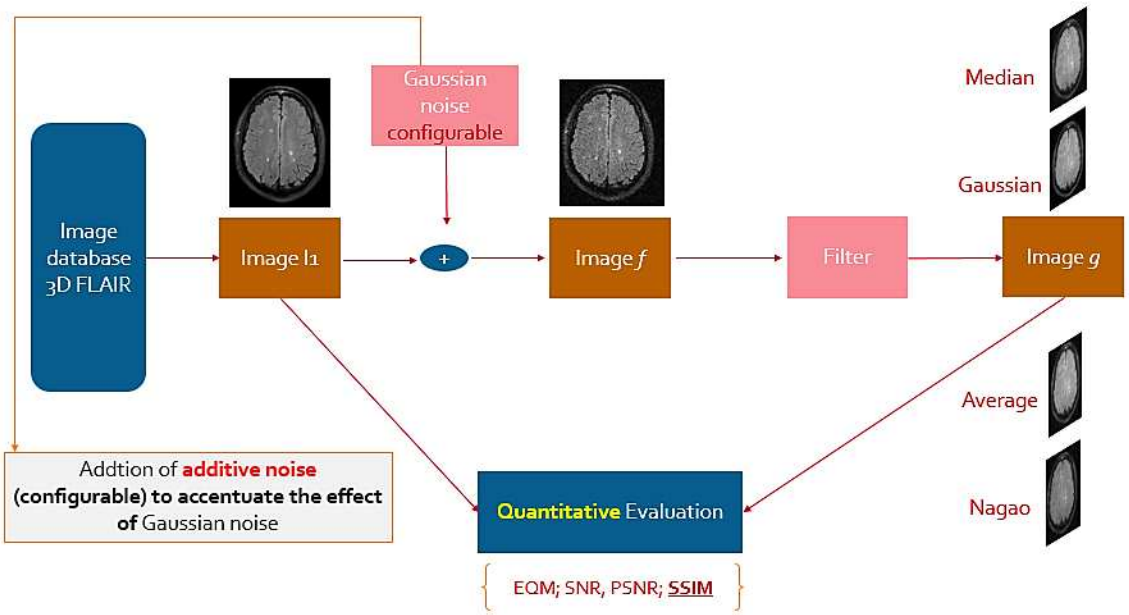

Fig 19. Workflow of Gaussian configurable noise addition

The structural similarity index (SSIM) is a criterion of similarity between two digital images. It measures the visual quality of a distorted (filtered) image, compared to the original image. The SSIM metric is calculated over

multiple windows of size MxN. It compares luminance, contrast and structure (objects AND/OR contours).The SSIM result varies between 0 and 1 (Fig.20).

$$SSIM = f(l, c, S) \tag{11}$$

Where l is luminance, c is contrast and S is structure

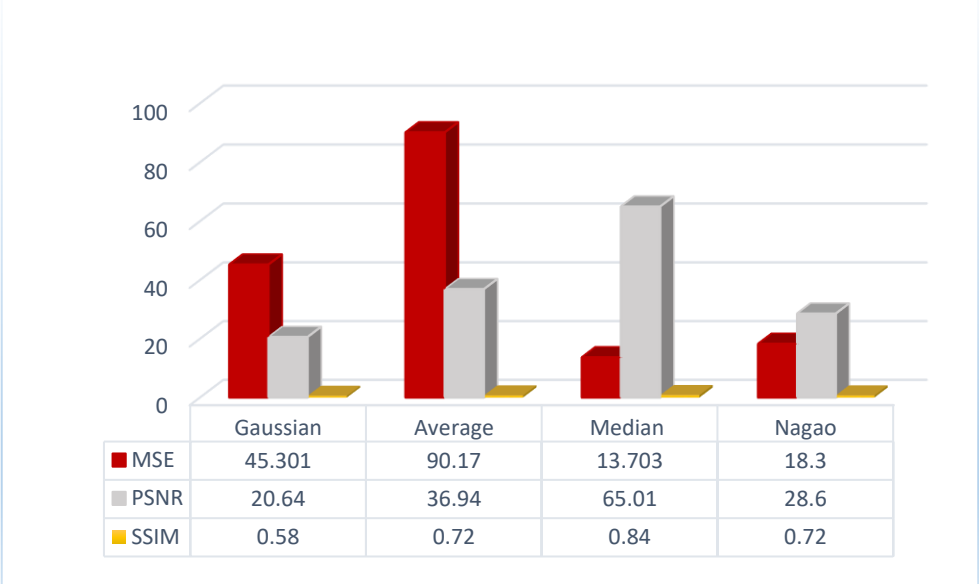

	Gaussian	Average	Median	Nagao
MSE	45.301	90.17	13.703	18.3
PSNR	20.64	36.94	65.01	28.6
SSIM	0.58	0.72	0.84	0.72

Fig 20. Filtering results= $f(MSE, PSNR, SSIM)$

Although the images were acquired with high resolution but interruptedly the MS lesions (which appear in hypersignal compared to the other parts of the brain) are not clear and differentiable compared to the related parts. This requires another preprocessing which is the contrast adjustment. Contrast "C" adjustment has been applied to all data base. For sufficient minimum contrast, the following conditions must be met: C ≥ 0.4 in general. C ≥ 0.7 for text or pictograms or to indicate sources of instability (see Fig.21).There are many definitions of contrast. One of the most known, the Michelson contrast **[29]** was introduced to allow a measure of the visibility of the interference fringes on test charts whose luminance varied sinusoidal from L_{min} at L_{max}.

The adjustment of contrast showed the improvement of the appearance of the lesions as well as their highlighting.

$$C^f = \frac{L_{\max} - L_{\min}}{L_{\max} + L_{\min}} \tag{12}$$

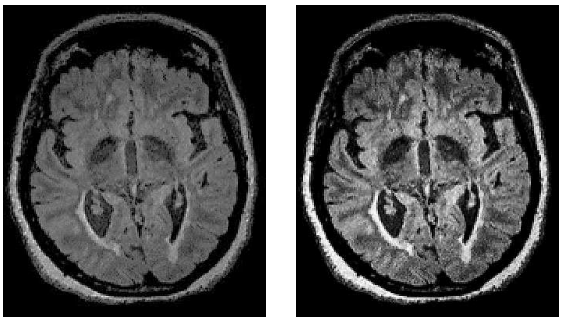

$C^f = 0{,}9841$ $C^f = 0{,}692$

Fig 21. Contrast calculation

Indeed, at this step, we can further refine the result obtained by eliminating the related parts of the brain (Fig.22) using the proposed approach of Dachraoui *et al*., **[34].** The study is based on mathematical morphology combined region growing.

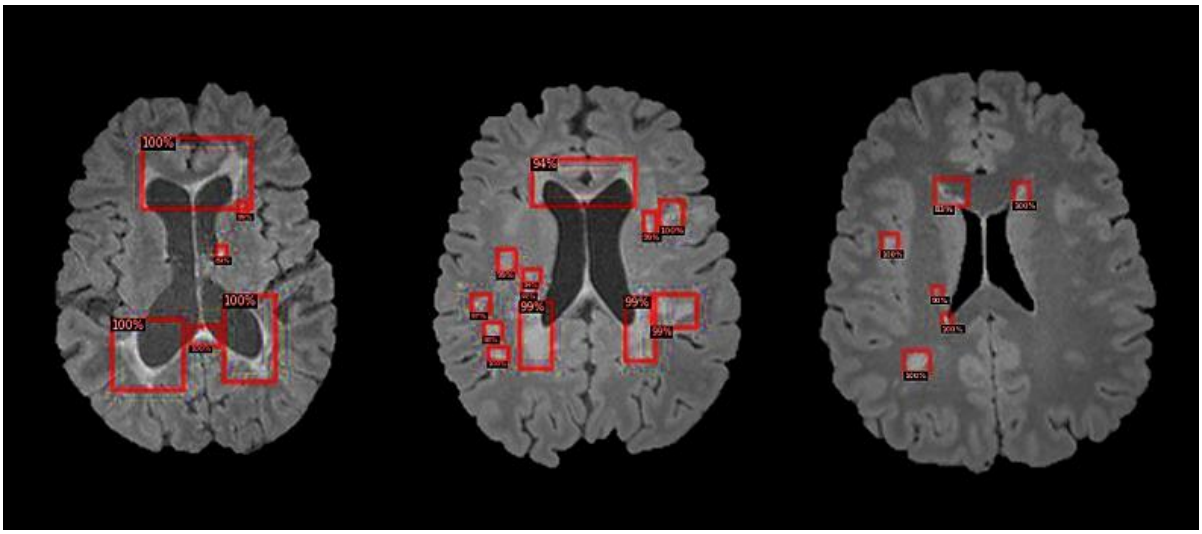

(a)

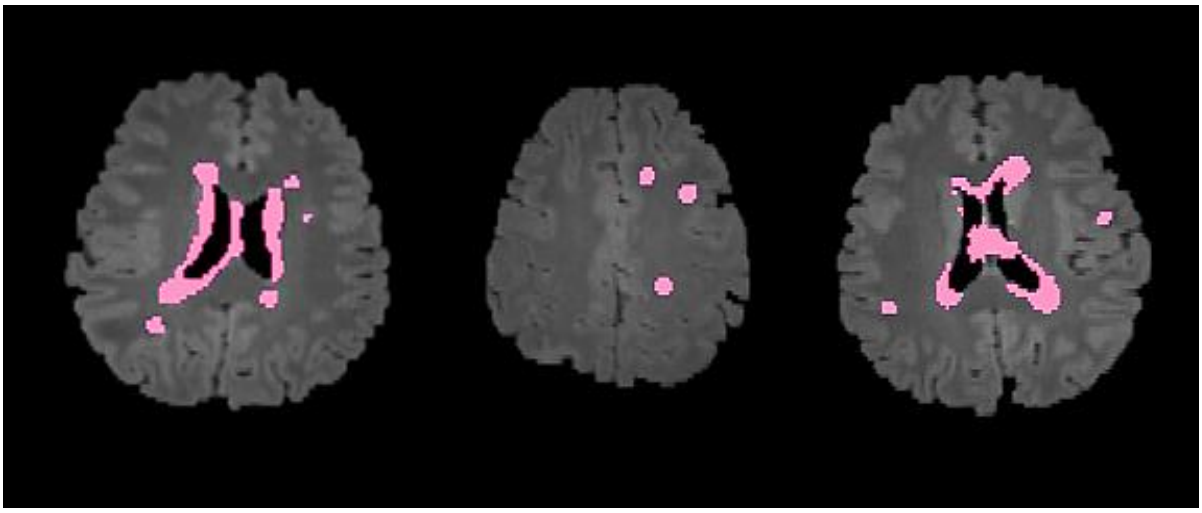

(b)

Fig 22. Refined results : a) Detection, b) segmentation

3.2. Prognosis

For the prognosis we have used three features precisely: the time series, the fractal dimension and the large Lyapunov exponent. The time series was presented in the phase space through marking the center of gravity inside the MS lesion, see figure 23. In fact, in this step, we can be limited to one MS lesion.

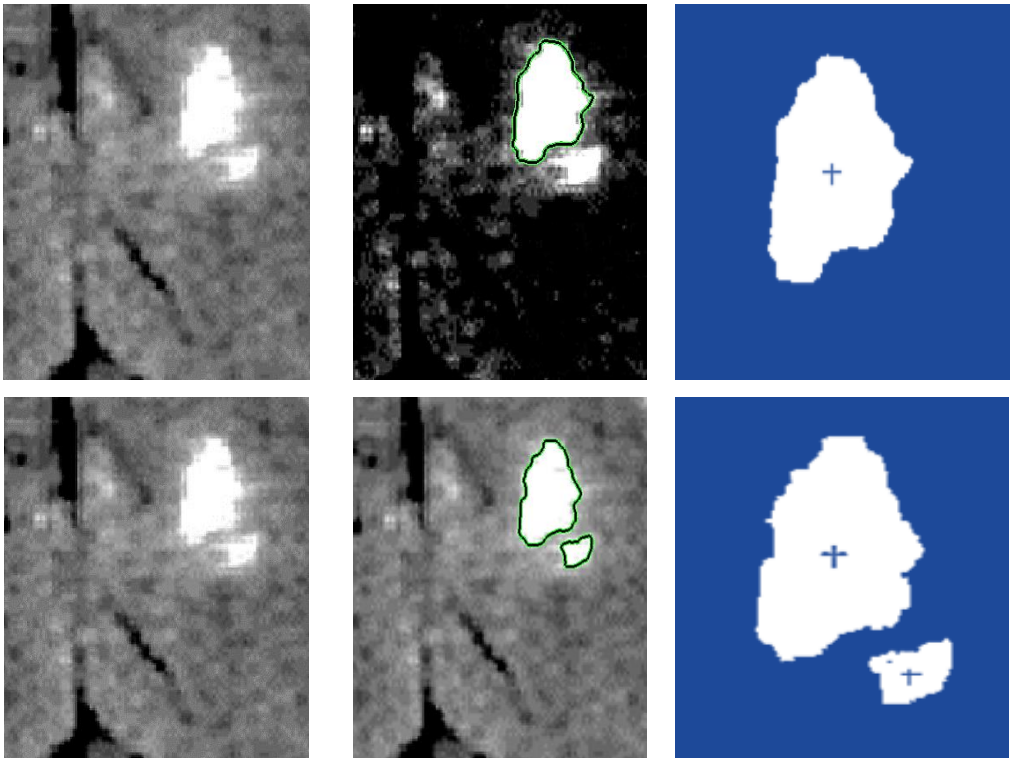

(a) **(b)** **(c)**

Fig 23. Delineation of the gravity center in MS lesion
a) Original image; b) lesions segmentation; c) post up the gravity center

Time series is presented in the phase space depending on the MS lesions shape (Fig.24). It is not uniform for all lesions.

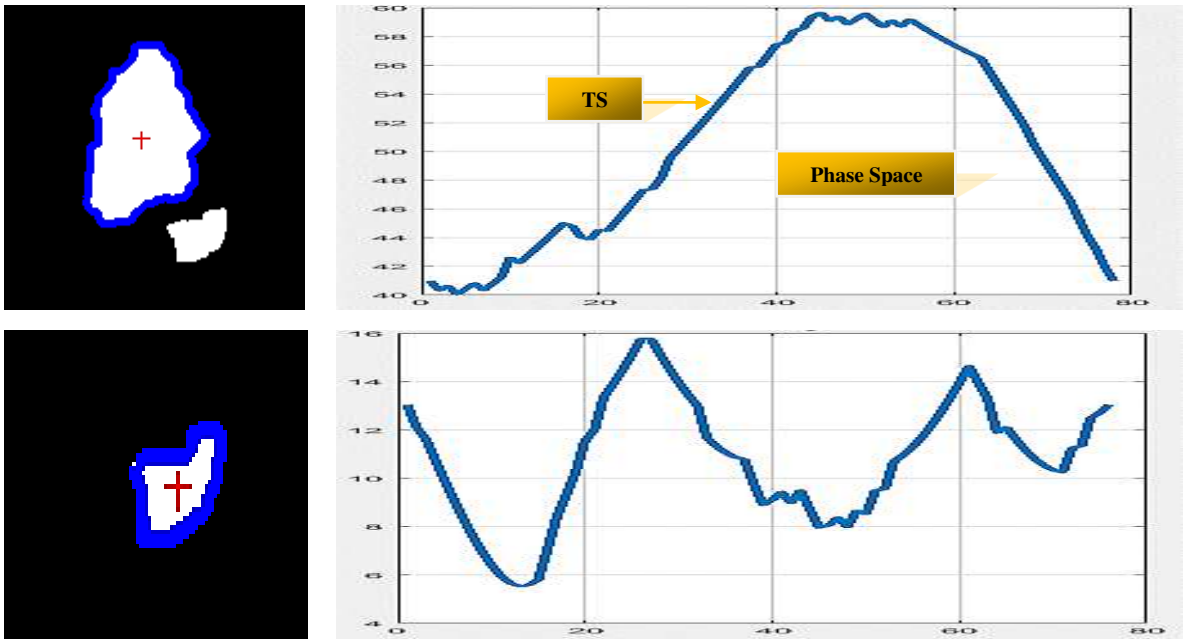

(a) **(b)**

Fig 24. Time series representation
a) Border delineation; b) time series representation in the phase space

The Fractal Dimension, FD, is calculated for the lesions presented above and is calculated from the extracted TS (Fig. 25).

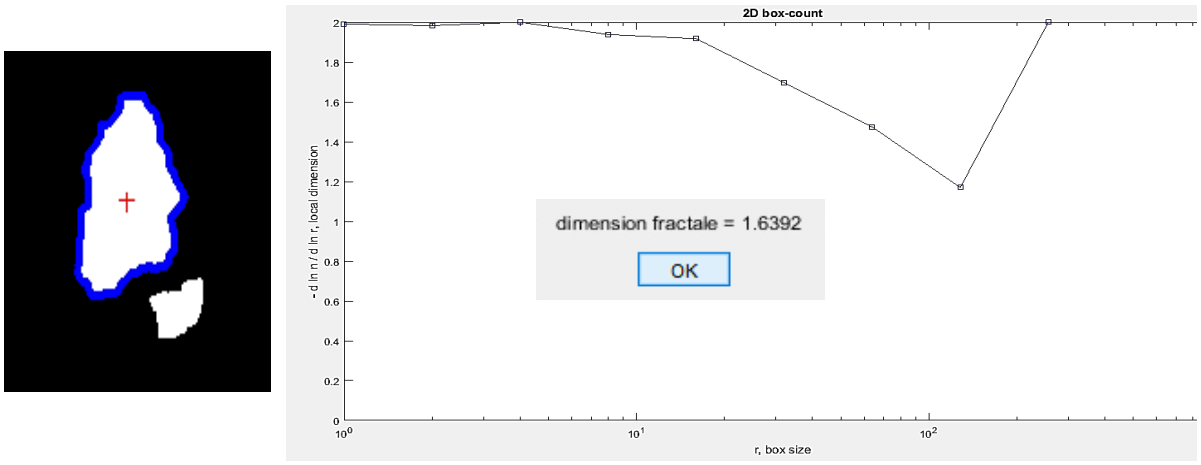

(a) **(b)**

Fig 25. 2D box count for fractal dimension: a) MS lesion; b) FD result

A series of Lyapunov exponent was calculated. Moreover, we will base essentially on the large exponent which is the most significant. The LLE is equal to 0.313007597967851. It is positive for this lesion.

After segmenting the lesion, the prognosis was applied based on the extraction of certain features: time series, fractal dimension and lyapunov spectrum.

The result of the temporal series depends uniquely on the shape of the lesion. There are two forms: a simple round or oval lesion with “flattened” and net contours called typical lesion, and a lesion with acute edges called atypical. This deformation has modified the number points of the TS representation in the phase space. More the contours are sharp, more the peaks increase in the TS curve (representing, thus, the good progress of our obtained results). Two motifs were generated by paint application to explain the difference between the TS curve (Fig.26).

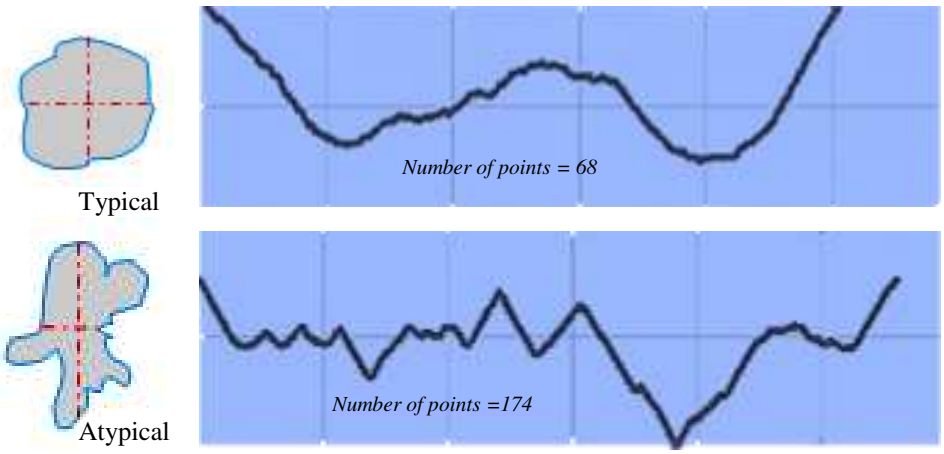

Fig 26. Typical and atypical lesions: a) Motifs, b) TS representation

The fractal dimension evenly changes according to the shape of the lesion. Atypical lesions have a higher FD than typical lesions as demonstrated in Fig. 26.The calculations were made on a set of 1000 typical lesions and 1000 atypical lesions, grouped every 200 images with their average FD (Fig.27).

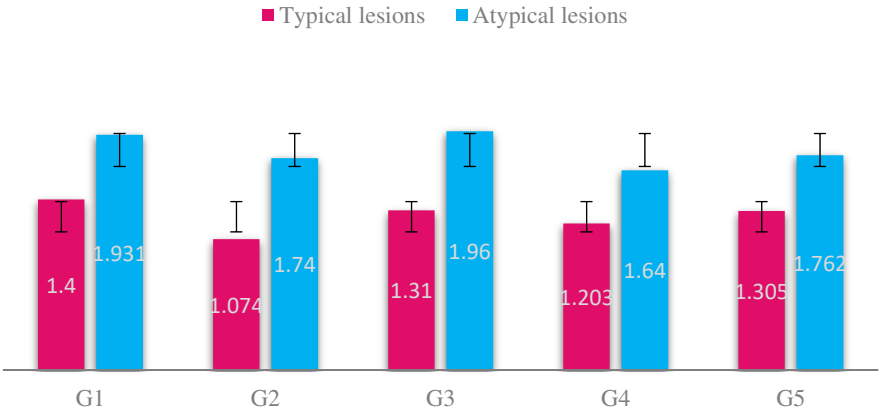

Fig 27. Fractal dimension distribution on a set of typical and atypical lesions

The Lyapunov spectrum is extracted from the time series. It was an interval between positive and negative values. Although we entirely relied on the large exponent which represents a significant value for lesion evolution as well as its future. Lesions with positive LLEs represent active lesions with an unpredictable evolution in space and time. The lesions called 'stagnated' had ~~a~~ negative values, meaning that the evolution has stopped either in space and time. In this context, two clinical cases from the National Institute Mongi Ben Hmida of Tunisia have been discussed in order to demonstrate this evolution probability.

For the 1st clinical case, the patient consults to assess the progression and the response of MR lesions following the initiation of a new disease-modifying treatment. The acquisitions are compared to the previous MRI of September 2, 2021. As a result, a new demyelinating FLAIR hyperintense lesions discreetly enhanced in the periphery, appeared since the previous examination and a stability of the lower left frontal oval lesion strongly enhanced compatible with a meningioma. The quantitative study for this case shows that MS lesions have a flattened time series devoiced from peaks and the average fractal dimension of the several lesions resented in the image is equal to 1.091. The large exponent extracted from the Lyapunov exponents spectrum is a negative value and equal to -3.703. The obtained results verify the proposed approach. The lesion will not evolve over time.

For the 2nd clinical case, the patient consults for strabismus and suspicion of MS disease. As a result, a hypersignals of the supratentorial white matter, not enhanced. They do not respond to McDonald's criteria for spatial and temporal dissipation and a non-specific appearance that requires comparison with histological, biological and clinical evolution data. For the quantitative study the presented lesions have a flattened time series with definite peaks and the fractal dimension of the lesion resented in the image is equal to 1.460. The large exponent extracted from the Lyapunov exponents spectrum is a negative value which tends to 0 (= -0.97403). In this clinical case, since this is his first MRI, the histological data is essentially absent, and no previous MRI acquisitions. Therefore,

we are essentially based on the quantitative study which estimate that the patient is suspect and at risk of unpredictable developments.

4. Conclusion

In this study, an autonomous and fast approach has been proposed to localize multiple sclerosis lesions and predict its evolution using Detecron-2 in 3D FLAIR MRI images. Our main focus consists on the identification of the different pre-processing phases, as well as on the optimal-configuration process for the proposed deep-learning model. The detailed detection and segmentation process and experiments for validation has been provided. Once the initial segmented lesions have been obtained, chaotic features was extracted from the phase space for each MS lesion that appears in hyperintense. For the proposed pipeline the results have been presented with a database of 150 patients. Four clinical cases were discussed pointing the difference between active lesions which explains a "poor" prognosis with respect to permanent lesions without evolution and which presents a good prognosis.

Chaos theory is used in several fields however few in medicine, especially in neuroradiology. The lesions evolution was purely based on spatial manifestations which are still insufficient to confirm the diagnosis. One of the primary limitations of the presented approach is the absence of supporting histological information, i.e. these clinical imaging data need to be compared with complementary histological data. Moreover, numerous hospitals do not have the PACS archiving system. Therefore, the data is deleted every 5 years in order to store else patients data. Furthermore we completely drop patient follow-up.

Funding declaration

The author(s) received no financial support for the research, authorship, and/or publication of this article.

Author Contribution

Material preparation, data collection and analysis were performed by [Chaima Dachraoui].

The first draft of the manuscript was written by [Chaima Dachraoui].

[Aymen Mouelhi], [Salam Labidi], [Amine Mosbeh], [Wassim Sliti] and [Basel Solaiman] commented on previous versions of the manuscript.

[Aymen Mouelhi], [Salam Labidi], [Amine Mosbeh], [Wassim Sliti] and [Basel Solaiman] read and approved the final manuscript.

All authors contributed to the study conception and design.

Conflict of interest statement

The authors declare that they have no known conflict of interest that could have appeared to influence the work reported in this paper.

Ethical approval statement

No consent was recommended for this medical research. Personal patient data was not included in the paper. These are anonymous images and well processed protecting the privacy of patients. It is a thesis work in collaboration with the national institute of neurology. We have no direct contact with the patients. The work took place purely in the doctors' reading room on anonymous acquisitions.

References

[1] R. Canani Sommer, J. Hata, C. de Medeiros Rimkus, B.Klein da Costa, J. Nakahara, D. Kazutoshi Sato, Mechanisms of myelin repair, MRI techniques and therapeutic opportunities in multiple sclerosis, Multiple Sclerosis and Related Disorders. 58 (2022). https://doi.org/10.1016/j.msard.2021.103407.

[2] C.Lubetzki, B. Zalc, A.Williams, C. Stadelmann, B. Stankoff, Remyelination in multiple sclerosis: from basic science to clinical translation, The Lancet Neurology. 19(8) (2020) 678-688. https://doi.org/10.1016/S1474-4422(20)30140-X.

[3] B. Cree, J. Oksenberg, S. Hauser, Multiple sclerosis: two decades of progress, The Lancet Neurology. 21(3) (2022) 211-214. https://doi.org/10.1016/S1474-4422(22)00040-0.

[4] on behalf of the MAGNIMS study group, MAGNIMS consensus guidelines on the use of MRI in multiple sclerosis—establishing disease prognosis and monitoring patients, Nature Reviews Neurology. 11 (2015) 597–606. https://doi.org/10.1038/nrneurol.2015.157.

[5] P. Rommer, U. Zettl, B. Kieseier, H. Hartung, T. Menge, E. Frohman, B. Greenberg, B. Hemmer, O. Stüve, Requirement for safety monitoring for approved multiple sclerosis therapies: an overview, Clinical and experimental immunology. 175(3) (2014) 397–407. https://doi.org/10.1111/cei.12206.

[6] P.Schmidt, V. Pongratz, P. Küster, D. Meier, J. Wuerfel, C. Lukas, B. Bellenberg, F. Zipp, S. Groppa, P. Sämann, F. Weber, C. Gaser, T. Franke, M.Bussas, J. Kirschke, C. Zimmer, B.Hemmer, M. Mühlau,Automated segmentation of changes in FLAIR-hyperintense white matter lesions in multiple sclerosis on serial magnetic resonance imaging, NeuroImage: Clinical. 23 (2019). https://doi.org/10.1016/j.nicl.2019.101849.

[7] C. Polman, S. Reingold, B. Banwell, M. Clanet, J. Cohen, M. Filippi, K. Fujihara, E. Havrdova, M. Hutchinson, L. Kappos, F. Lublin, X. Montalban, P. O'Connor, M. Sandberg-Wollheim, A. Thompson, E. Waubant, B. Weinshenker, J. Wolinsky, Diagnostic criteria for multiple sclerosis: 2010 revisions to the McDonald criteria. Annals of neurology, 69(2) (2011) 292–302. https://doi.org/10.1002/ana.22366.

[8] A. Thompson, B. Banwell, F.Barkhof, W.Carroll, T. Coetzee, G. Comi, J. Correale, F. Fazekas, M. Filippi, M. Freedman, K. Fujihara, S. Galetta, H. Hartung, L. Kappos, F. Lublin, R. Marrie, A. Miller, D. Miller, X. Montalban, E. Mowry, P. Sorensen, M. Tintoré, A. Traboulsee, M. Trojano, B. Uitdehaag, S. Vukusic, E. Waubant, B. Weinshenker, S. Reingold, J. Cohen, Diagnosis of multiple sclerosis: 2017 revisions of the McDonald criteria, The Lancet Neurology. 17(2) (2018) 162-173. https://doi.org/10.1016/S1474-4422(17)30470-2.

[9] C. Dachraoui, A. Mouelhi, C. Drissi, S. Labidi, (2022) Automated Diagnosis of Multiple Sclerosis Lesions in Brain MRI Using 3D-FLAIR Acquisition. In Proceedings of Sixth International Congress on Information and Communication Technology (pp. 1-8). Springer, Singapore.

[10] S. Ansari, K. Javed, S. Qaisar, R. Jillani, U. Haider, Multiple Sclerosis Lesion Segmentation in Brain MRI Using Inception Modules Embedded in a Convolutional Neural Network, Journal of Healthcare Engineering. 10 (2021) 1-10. https://doi.org/10.1155/2021/4138137.

[11] S. Valverde, M. Cabezas, E. Roura, S. González-VilLA, D. Pareto, J. Vilanova, L. Ramió-Torrentà, A. Rovira, A. Oliver, X. Lladó, Improving automated multiple sclerosis lesion segmentation with a cascaded 3d convolutional neural network approach, NeuroImage. 155 (2017) 159–168. https://doi.org/10.1016/j.neuroimage.2017.04.034.

[12] F. La Rosa, A. Abdulkadir, M. João Fartaria, R. Rahmanzadeh, P. Jui Lu, R. Galbusera, M. Barakovic, J. Thiran, C. Granziera, M. Cuadra, Multiple sclerosis cortical and WM lesion segmentation at 3T MRI: a deep learning method based on FLAIR and MP2RAGE, NeuroImage: Clinical. 27 (2020). https://doi.org/10.1016/j.nicl.2020.102335.

[13] C. Dachraoui, A. Mouelhi, C. Drissi, S. Labidi, (2020) Predictive Approach of Multiple Sclerosis MR-Lesions Evolution based on Chaotic Attributes. In 7th International Conference on Control, Decision and Information Technologies (CoDIT), (pp. 265-270), https://doi.org/10.1109/CoDIT49905.2020.9263901.

[14] V. Gupta, M. Mittal, Chaos Theory: An Emerging Tool for Arrhythmia Detection. Sensing and Imaging. 21 (2020) 1-22. https://doi.org/10.1007/s11220-020-0272-9.

[15] F. Denis, C. Letellier, Chaos theory: a fascinating concept for oncologists. Cancer Radiotherapie, Journal de la Societe Francaise de Radiotherapie Oncologique. 16(3) (2012) 230-236. https://doi.org/10.1016/j.canrad.2012.01.003.

[16] T. Akaishi, T. Takahashi, I. Nakashima, Chaos theory for clinical manifestations in multiple sclerosis, Medical hypotheses. 115 (2018) 87–93. https://doi.org/10.1016/j.mehy.2018.04.004.

[17] S. Berhil, H. Benlahmar, N. Labani, A review paper on artificial intelligence at the service of humanresources management, Indonesian Journal of Electrical Engineering and Computer Science. 18(1) (2020) 32-40. http://doi.org/10.11591/ijeecs.v18.i1.pp32-40.

[18] K. He, G. Gkioxari, P. Dollár, R. Girshick, Mask R-CNN, (2017). In IEEE International Conference on Computer Vision (ICCV), pp. 2980-2988. http://doi.org/10.1109/ICCV.2017.322.

[19] https://ai.facebook.com/blog/-detectron2-a-pytorch-based-modular-object-detection-library-/.Accessed March 19, 2022.

[20] B. Goyal, A. Dogra, S. Agrawal, B. Sohi? Noise Issues Prevailing in Various Types of Medical Images, Biomedical and Pharmacology Journal. 11(3) (2018). https://dx.doi.org/10.13005/bpj/1484.

[21] C. Shorten, T. Khoshgoftaar, A survey on image data augmentation for deep learning. Journal of big data. 6(1) (2019) 1-48. https://doi.org/10.1186/s40537-019-0197-0.

[22] J. Long, E. Shelhamer, T. Darrell, Fully convolutional networks for semantic segmentation (2015). In IEEE Conference on Computer Vision and Pattern Recognition (CVPR), Boston, MA, USA, pp. 3431-3440. https://doi.ieeecomputersociety.org/10.1109/CVPR.2015.7298965.

[23] C. Oestreicher, A history of chaos theory. Dialogues in Clinical Neuroscience. 9(3) (2007) 279-289. https://doi.org/10.31887/DCNS.2007.9.3/coestreicher.

[24] S. Kesić, Systems biology, emergence and antireductionism. Saudi journal of biological sciences. 23(5) (2016) 584–591. https://doi.org/10.1016/j.sjbs.2015.06.015.

[25] A. Basharat, M. Shah, Time series prediction by chaotic modeling of nonlinear dynamical systems (2009). In IEEE 12th International Conference on Computer Vision, pp. 1941-1948. https://doi.org/10.1109/ICCV.2009.5459429.

[26] Y. Shon, The Pattern Recognition System Using the Fractal Dimension of Chaos Theory, The International Journal of Fuzzy Logic and Intelligent Systems. Korean Institute of Intelligent Systems (2015). https://doi.org/10.5391/ijfis.2015.15.2.121.

[27] Y. Liu, L. Chen, H. Wang, L. Jiang, Y. Zhang, J. Zhao, D. Wang, Y. Zhao, Y. Song, An improved differential box-counting method to estimate fractal dimensions of gray-level images, Journal of Visual Communication and Image Representation. 25(5) (2014) 1102-1111. https://doi.org/10.1016/j.jvcir.2014.03.008.

[28] G. Zhang, Y. Pan, L. Zhang, Deep learning for detecting building façade elements from images considering prior knowledge, Automation in Construction. 133 (2022). https://doi.org/10.1016/j.autcon.2021.104016.

[29] J. Dain, C. Bridge, M. Relf, A. Lukman, S. Manandhar, M. Boon, Issues in specifying contrast in building elements for people with a visual disability. Work. 70(4) (2021) 1219-1227. https://doi.org/10.3233/WOR-205158.

[30] S. Roy, J. A. Butman, L. Chan, D. L. Pham, TBI contusion segmentation from MRI using convolutional neural networks (2018). In IEEE 15th International Symposium on Biomedical Imaging (ISBI) pp. 158-162. https://doi.org/10.1109/ISBI.2018.8363545.

[31] S. Valverde, M. Cabezas, E. Roura, S. González-Villa, J. Salvi, A. Oliver, Multiple sclerosis lesion detection and segmentation using a convolutional neural network of 3D patches, MSSEG Challenge Proceedings: Multiple Sclerosis Lesions Segmentation Challenge Using a Data Management and Processing Infrastructure 75 (2016) 84-88.

[32] S. Valverde, M. Salem, M. Cabezas, D. Pareto, J. Vilanova, L. Ramió-Torrentà,, A. Rovira, J. Salvi, A. Oliver, X. Lladó, One-shot domain adaptation in multiple sclerosis lesion segmentation using

convolutional neural networks, NeuroImage Clinical. 21 (2019). https://doi.org/10.1016/j.nicl.2018.101638.

[33] S. Aslani, M. Dayan, L. Storelli, M. Filippi, V. Murino, M. Rocca, Multi-branch convolutional neural network for multiple sclerosis lesion segmentation, NeuroImage. 196 (2019) 1-15. https://doi.org/10.1016/j.neuroimage.2019.03.068.

[34] C. Dachraoui , A. Mouelhi, C. Drissi, S. Labidi, Chaos theory for prognostic purposes in multiple sclerosis, Transactions of the Institute of Measurement and Control. (2021). https://doi.org/10.1177/01423312211040309.